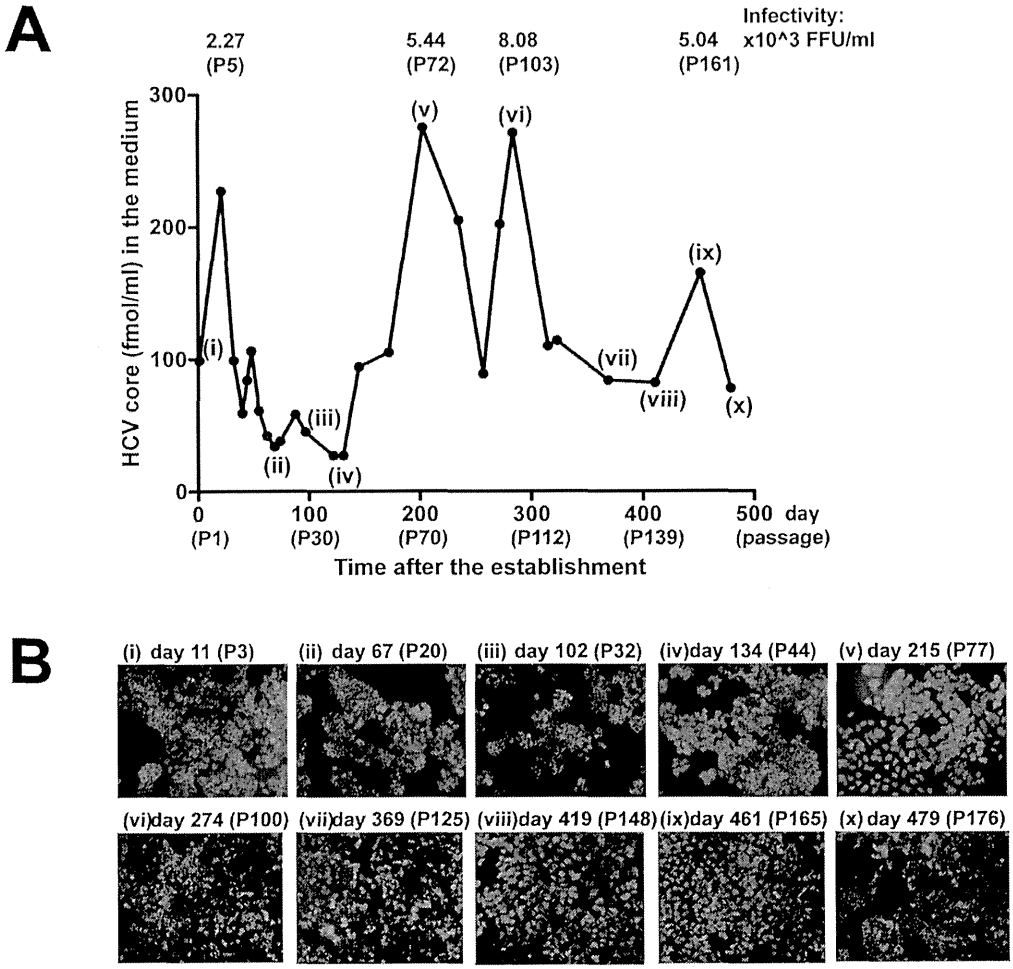

Figure 2. HPI cells supported HCV infection more than a year after establishment. (**A**) HCV core protein concentration in the medium was determined after the establishment of HPI cell. At time points indicated in Roman numerals, immunofluorescence staining for HCV was performed (B). Infectivity of HCVcc in the medium is shown above the graph. P-numbers in parentheses represent passage numbers after the establishment of HPI cell. (**B**) Immunofluorescence staining for HCV NS5A protein in the cells was performed.
doi:10.1371/journal.pone.0094460.g002

ATP (Table 1) were noted in HPI cells. Both metabolites are known to facilitate this reaction. Moreover, a rate-limiting enzyme for this pathway is hydroxymethylglutaryl-CoA reductase (HMGCR), which was up-regulated (Figure 4A, B). In addition, other enzymes such as acetyl-CoA acetyltransferase 1 (ACAT1), hydroxymethylglutaryl-CoA synthase 1 (HMGCS1), and squalene epoxidase (SQLE) were moderately upregulated in transcription (Figure 4A), seemingly contributing to the cholesterol increase.

Actual level of cholesterol was increased in the HPI cell (Figure 4A) supporting the aforementioned biochemical data (Figure 3B). Interestingly, not only an increase of cholesterol but also a drastic increase of desmosterol, a cholesterol precursor, was remarkable in HPI cells (Figure 4A). Desmosterol is converted from 7-dehydrodesmosterol by 7-dehydrocholesterol reductase (DHCR7), which was not up-regulated in HPI cell (Figure 4A, B). Rather up-regulation of sterol-5-desaturase (SC5DL) gene, upstream of DHCR7, might be attributed to the increase in desmosterol (Figure 4A). Taken together, we found that the cholesterol biosynthetic pathway was facilitated in HPI cells with up-regulation of the rate-limiting enzyme, HMGCR, and the related genes.

Increased Fatty Acid Pool

Next, we analyzed the biosynthetic pathways of fatty acids and triacylglycerol, the other major component of LD (Figure 5A). At first, cytosolic acetyl CoA is converted to malonyl CoA, and then, through multiple steps, to palmitic acid, an initial fatty acid of this pathway. Longer fatty acids are sequentially generated from palmitic acid by elongation-of-very-long-chain-fatty-acids enzymes (ELOVLs). Meanwhile, generated fatty acids are desaturated by the formation of carbon double bonds, resulting in variety of fatty acids, fatty acid pool. Up-regulation of a rate-limiting enzyme for this pathway, acetyl-CoA carboxylase α (ACACA), was noted at protein level in HPI cells (Figure 5A, B). Moderate up-regulation of the elongation enzymes, ELOVL5 and ELOVL6, and the desaturation enzymes, stearoyl-CoA desaturase (SCD), was also noted (Figure 5A). Of them, the increase of only ELOVL5 was confirmed at the protein level (Figure 5B). Resultantly, various fatty acids were remarkably increased, indicating that HPI cells were rich in fatty acid pool (Figure 5C).

In following steps, triacylglycerol is synthesized by the addition of three molecules of acyl-CoA, which are generated from fatty acids, to one molecule of glycerol 3-phosphate. The addition of the first acyl-CoA to glycerol 3-phosphate is catalyzed by glycerol-3-

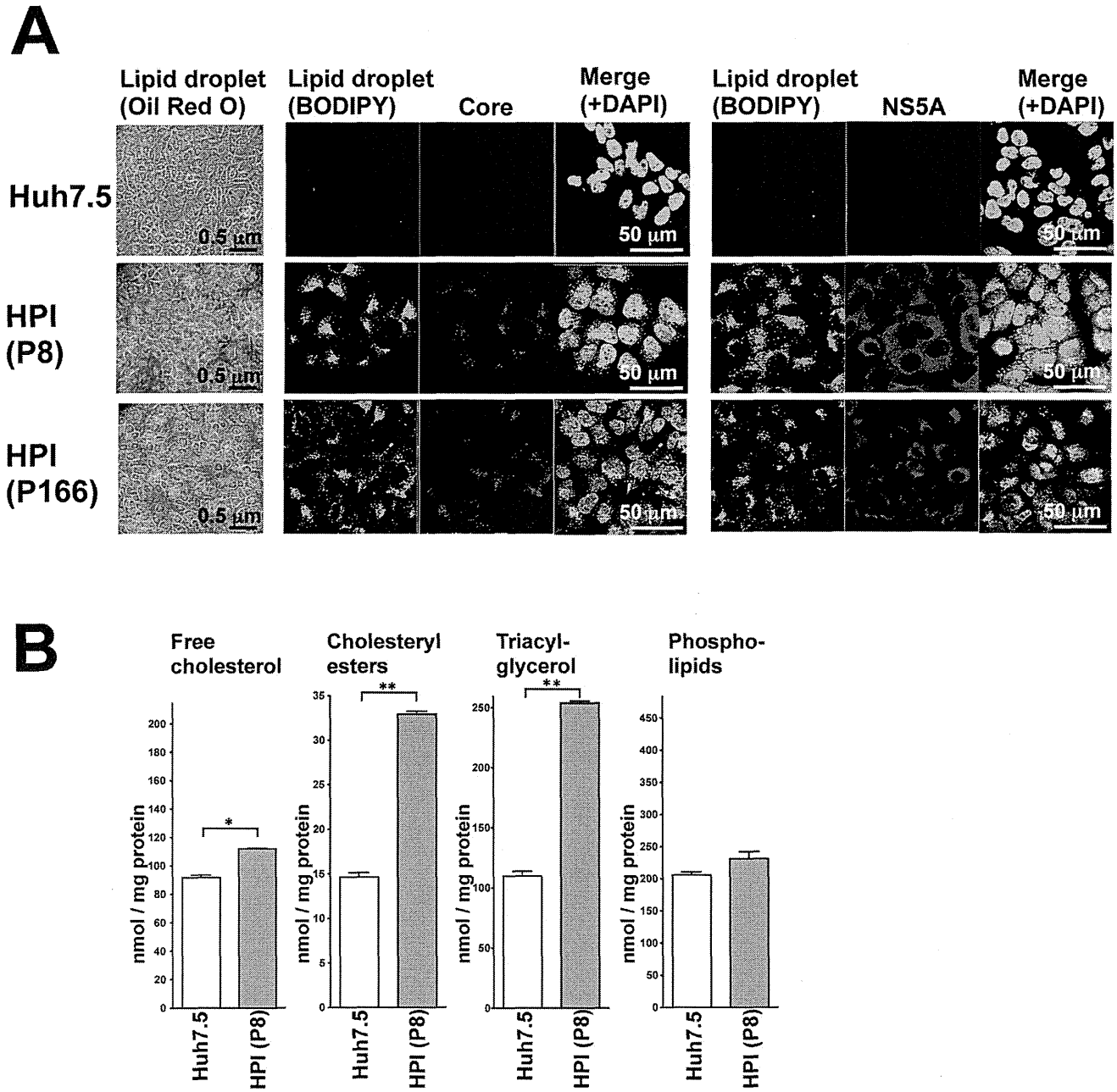

Figure 3. Remarkable accumulation of lipid droplets in HPI cells. (**A**) Huh7.5 cells and HPI cells at passages 8 and 166 were stained with Oil Red O for LDs (dark red) and observed with a light microscope (most left panels). They were also subjected to confocal laser scanning microscopy after immunofluorescence staining for LDs with BODIPY and for HCV core and NS5A proteins. Green fluorescence represents LDs (2nd and 5th panels from the left) and red fluorescence represents the HCV core (3rd panels from the left) and NS5A (6th panels from the left). Their images were merged with nuclei counterstained by DAPI (4th and 7th panels from the left), where the yellow areas indicate colocalization of LD with HCV proteins. The enlarged images were shown in Figure S3. (**B**) Intracellular lipid contents in Huh7.5 cells and HPI cells at passage 8 were determined in triplicate. Values were corrected by the protein concentration and statistically evaluated by Student's *t*-test indicating a significance of $P<0.001$ (*) and $P<0.0001$ (**).

doi:10.1371/journal.pone.0094460.g003

phosphate acyltransferase (GPAM), the expression of which was moderately up-regulated in HPI cells (Figure 5A, B). The addition of the third acyl-CoA is catalyzed by diglyceride acyltransferase (DGAT) 1 and 2. DGAT1 works predominantly for very low-density lipoprotein (VLDL) formation [18]. Thus, down-regulation of DGAT1 gene in HPI cell (Figure 5A) might have resulted in LD accumulation by reducing VLDL release. In addition, microsomal triglyceride transfer protein (MTTP) is involved in VLDL assembly and release [18] [19]. In HPI cell, down-regulation of MTTP was also noted (Figure 5A, B), probably also reducing VLDL release. On the other hand, patatin-like phospholipase domain-containing protein 3 (PNPLA3), which catabolizes triacylglycerol, was moderately up-regulated (Figure 5A, B) and hepatic lipase (LIPC), which is secreted from the cell and degrades extra-cellular triacylglycerol to free fatty acids for intake, was down-regulated (Figure 5A), suggesting negative feedback against

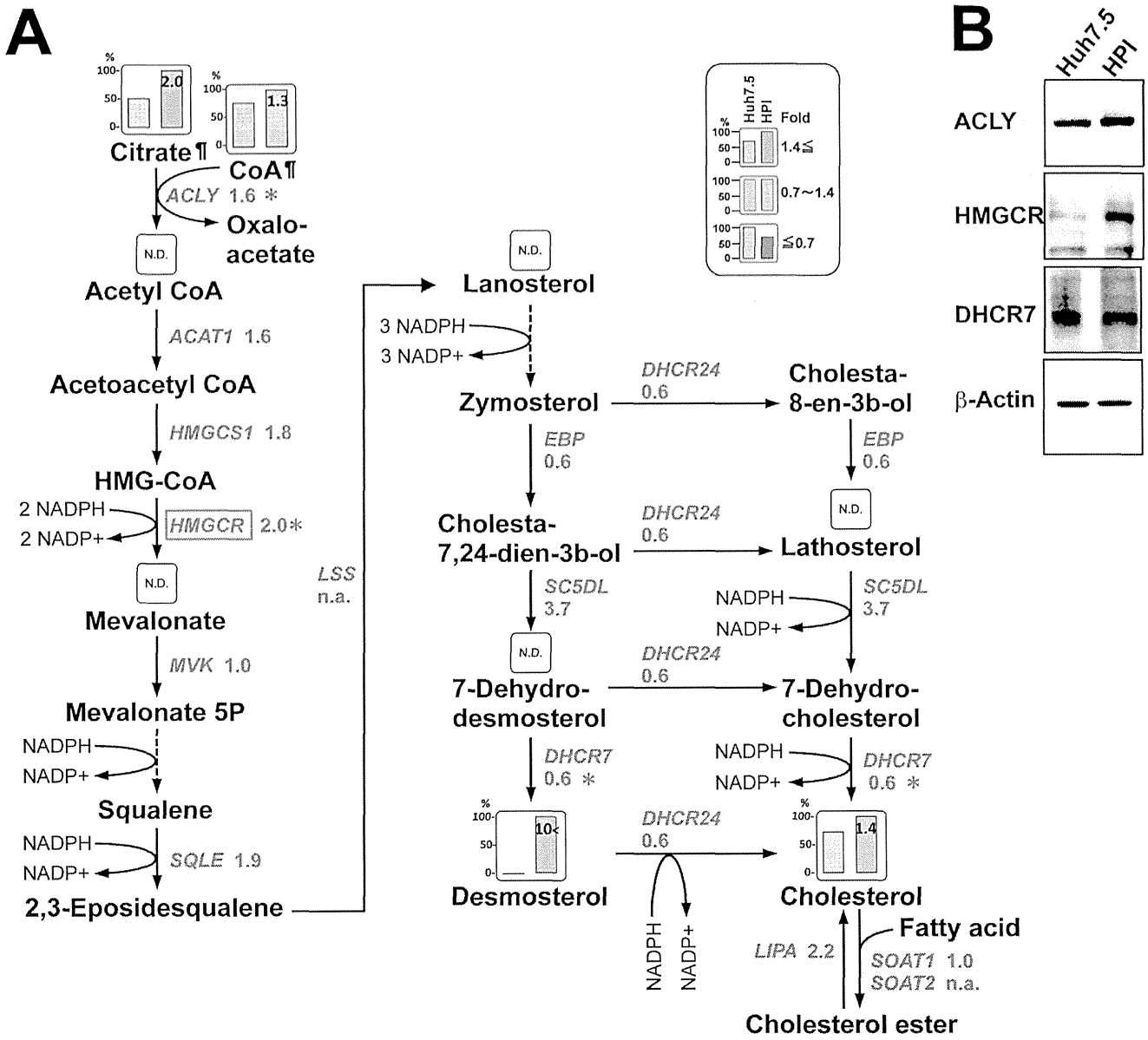

Figure 4. Biosynthetic pathway of cholesterol. (**A**) Relative quantities of metabolites in Huh7.5 (left column) cells and HPI cells (right column) are superimposed on a metabolic map of the cholesterol biosynthesis pathway according to the data (Table S1, Table S2). The metabolic map is depicted based on KEGG pathways (http://www.genome.jp/keg/). The NADPH/NADP+ reaction, if associated, was added to the main reaction. Height of column with larger quantity is set to 100%, and that of smaller quantity are shown proportionally. Numbers on the right columns indicate the fold-change of HPI compared to Huh7.5, and the color of the column represents: yellow (> = 1.4-fold), blue (= <0.7-fold), or gray (0.7~1.4-fold). ¶: A metabolite appearing on other figure. Genes (italicized) located between metabolites encode enzyme(s) for a corresponding reaction with fold-expressions of HPI to Huh7.5 according to the data (Table S3). A gene encoding a rate-limiting enzyme is surrounded by a square. *: Immunoblot analysis was also done for confirmation in (B). N.D.: Not detected. n.a.: Not assessed because of low expression. (**B**) Immunoblot analysis of the selected enzymes. Beta-actin was used as a control.
doi:10.1371/journal.pone.0094460.g004

the excess accumulation of LDs. Taken together, biosynthesis pathway of fatty acid and triacylglycerol was facilitated in HPI cells with up-regulation of the rate-limiting enzyme, ACACA, and down-regulation of genes to inhibit VLDL release.

Facilitation of the Pentose Phosphate Pathway, Purine Synthesis Pathway, and Serine Synthesis Pathway

Then we analyzed the glycolysis pathway because it is at a center of metabolisms followed by the tricarboxylic acid (TCA) cycle. As a first step, extracellular glucose is taken up into a cell and is converted to glucose-6-phosphate (G6P), whose level did not increase much in HPI cells (Figure 6A). Nor, glucokinase (GCK), a rate-limiting enzyme for this step, was not up-regulated at least in the protein level (Figure 6B). Nonetheless, three immediate intermediates of G6P increased remarkably: glucose-1-phosphate, 6-phosphogluconic acid, and fructose 6-phosphate, which lead to glycogenesis, pentose phosphate pathway (PPP), and glycolysis, respectively (Figure 5A). Level of most metabolites in glycolysis did not change or even decreased except for increase in pyruvate, a final product (Figure 6A). Expression of glyceraldehyde-3-phos-

Table 1. Intracellular concentration of nucleotides.

Metabolite	Huh7.5	HPI	Fold:
	pmol/10^6 cells	pmol/10^6 cells	HPI/Huh7.5
Purine metabolism			
IMP	N.D.	N.D.	N.A.
Adenosine	3.8	6.8	1.8
Adenine	15	17	1.1
AMP	110	239	2.2
ADP	1,144	1,758	1.5
ATP	9,358	14,551	1.6
dATP	30	38	1.3
cAMP	35	25	0.7
Gaunosine	N.D.	N.D.	N.A.
GMP	44	98	2.2
GDP	335	561	1.7
GTP	1,975	3,389	1.7
Pyrimidine metabolism			
dTMP	N.D.	N.D.	N.A.
dTTP	85	98	1.2
Cytidine	4.7	11	2.3
CMP	32	41	1.3
CDP	123	156	1.3
CTP	2,209	2,465	1.1
dCTP	86	71	0.8
Uridine	N.D.	N.D.	N.A.
UMP	166	219	1.3
UDP	343	532	1.6
UTP	5,429	6,595	1.2

N.D.: Not detected.
N.A.: Not available.
doi:10.1371/journal.pone.0094460.t001

phate dehydrogenase (GAPDH) did not differ (Figure 6A, B) as often used as a control for expression analysis. These results indicated glycolysis pathway was not facilitated in HPI cells as a whole.

PPP, an alternative pathway of glycolysis, supplies NADPH for reductive biosynthesis of cholesterol and fatty acids as well as for reduction of reactive oxygen species (ROS), and also supplies pentose for the following purine synthesis. In HPI cells, 6-phosphogluconate (6PG), an initial intermediate of the PPP, and sedoheptulose-7-phosphate (S7P) were remarkably increased (Figure 6A). Glucose-6-phosphate dehydrogenase (G6PD) is a rate-limiting enzyme for the PPP to catalyze G6P to 6PG in association with NADPH production. Of note, the G6PD was up-regulated drastically (6.8-fold) (Figure 6A, B), and actual level of NADPH was increased in HPI cells (Table 2).

In purine synthesis pathway, ribose 5-P (R5P) is synthesized through the PPP and converted to phosphoribosyl pyrophosphate (PRPP), which is catabolized to inosine monophosphate (IMP) and finally to purines, AMP and GMP. In HPI cells, the level of PRPP was increased with up-regulation of phosphoribosyl pyrophosphate amidotransferase (PPAT), its rate-limiting enzyme, and methylenetetrahydrofolate dehydrogenase 2 (MTHFD2) (Figure 6A, B). In fact, the level of AMP and GMP increased remarkably together with an increase in other purines; ADP, ATP, GDP, and GTP (Table 1). Moreover, *o*-phosphoserine, glycine, and threonine in serine synthetic pathway, another alternative pathway of glycolysis, were remarkably increased in HPI cell, although the increase of serine *per se* was small (Figure 6A). Taken together, although glycolysis pathway was not facilitated, its alternative pathways including the pentose phosphate pathway, purine synthesis, and serine synthesis were facilitated in HPI with actual increase in NADPH and purines.

Facilitation of the TCA Cycle and Increase in Amino Acids

Cytosolic pyruvate is transferred into the mitochondria, and, by the action of the pyruvate dehydrogenase complex, is converted to acetyl-CoA as a starting material for the TCA cycle. One subunit of this complex, dihydrolipoamide S-acetyltransferase (DLAT), was up-regulated in HPI cells (Figure 7A, B). As a whole, TCA cycle was facilitated with remarkable increase in citrate, *cis*-aconitate, 2-oxyglutarate, fumarate, and malate (Figure 7A). TCA cycle produces most of ATPs, actual level of which was increased in HPI cells (Table 1). Interestingly, phosphoenolpyruvate carboxykinase 2 (PCK2) gene, a rate-limiting enzyme for gluconeogenesis, was up-regulated in HPI cell (Figure 7A, B) and actually we confirmed increased glucose release from HPI cell (data not shown). Moreover, the expression of ME1, which produces NADPH, from malate in TCA cycle, was up-regulated in

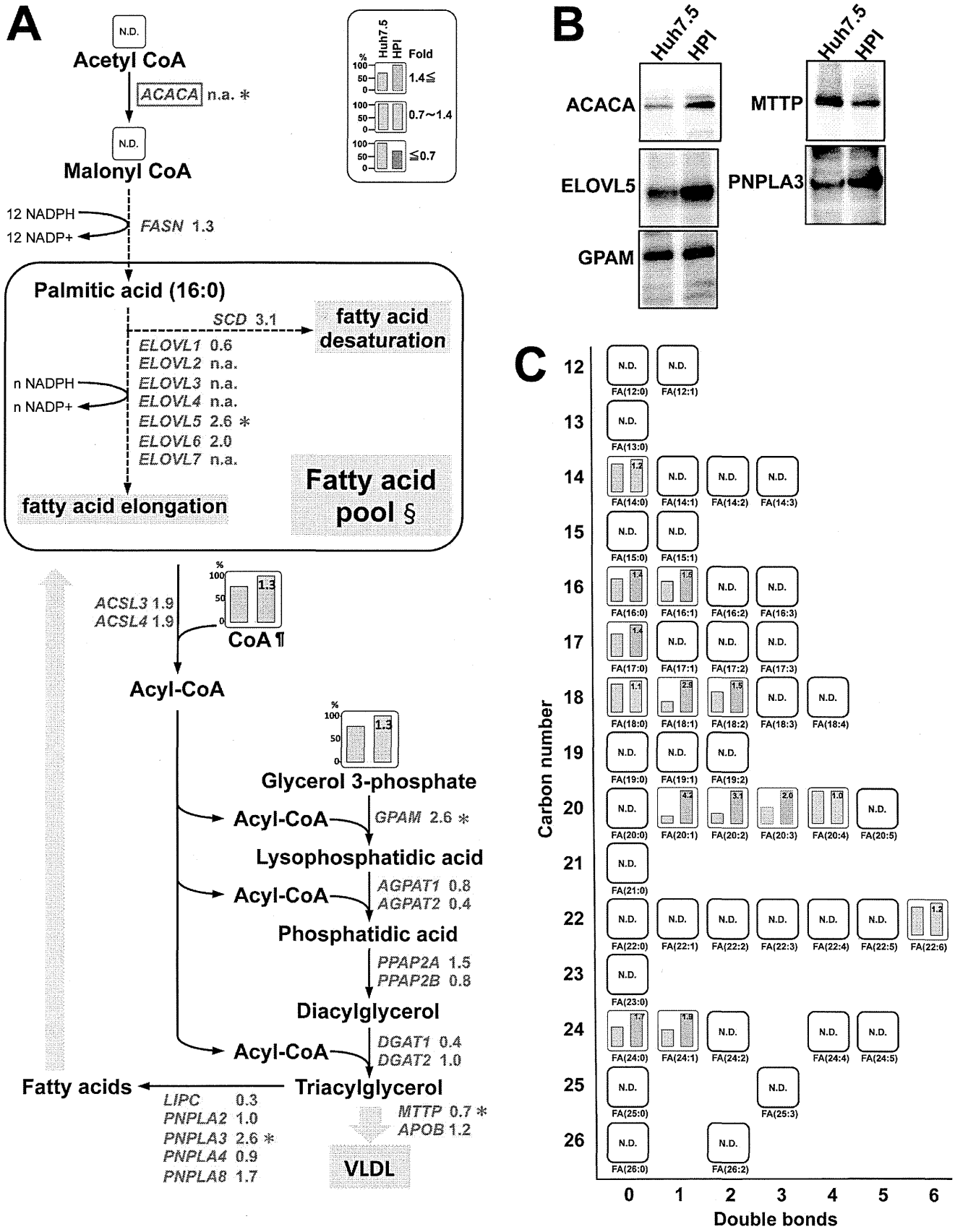

Figure 5. Biosynthetic pathway of fatty acids and triacylglycerol. (**A**) A metabolic map of fatty acids and triacylglycerol with gene expression is depicted in the same way as in Figure 4A. Symbols (¶, *, N.D., n.a.) represent the same meaning as in Figure 4A. §: Detailed content of individual

fatty acids in the fatty acid pool are shown in (C). (**B**) Immunoblot analysis of the selected enzymes. The control was the same beta-actin as in Figure 4B. (**C**) Relative quantity of fatty acids in the fatty acid pool is represented in order of the number of carbons (Y-axis) and the number of double bonds (X-axis).
doi:10.1371/journal.pone.0094460.g005

HPI cells (Figure 7A, B), suggesting contribution of ME1 in NADPH production together with the facilitated PPP.

Surprisingly, most of the essential amino acids were elevated; leucine, lysine, and tryptophan, histidine, isoleucine, valine, methionine, threonine, and phenylalanine (Figure 7A), speculating increased uptake of amino acids form outside of the cells since not all of them can be synthesized in human cells. Levels of non-essential amino acids, i.e., glutamate, tyrosine, aspartate (Asp), asparagine (Asn), arginine and alanine, were remarkably elevated in HPI cells, with only exception of decrease in glutamine (Figure 7A), indicating enhanced production of non-essential amino acids in association with the facilitation of TCA cycle,

Remarkable increase of Asp, which is catabolized from oxaloacetate in the TCA cycle, seems to have enhanced the urea cycle, since levels of argininosuccinate, arginine and citrulline were increased actually (Figure 7A). Increase of this amino acid might have caused also increase in N-acetylaspartate, N-carbamoyl aspartate, Asn and β-alanine (Figure 7A). Moreover, increase in Asn, converted from Asp coupled with the conversion of glutamine to glutamate, might be caused by up-regulation of its catalyzing enzyme asparagine synthetase (ASNS) (Figure 7A, B). Taken together, the TCA cycle was remarkably facilitated and maintained HPI cells in a hypermetabolic status with a marked increase in most of the amino acids and ATP.

Transactivation of Genes under Control of the Transcription Complex Nrf2/Maf-G

Intriguingly, of the genes up-regulated in the present study, G6PD, MTHFD2, ASNS, ME1, and PCK2 belong to an array of genes under the control by the transcription factor complex, Nrf2/Maf[11–14]. Therefore, additionally we examined expression of antioxidant and detoxification genes, NAD(P)H dehydrogenase quinone 1 (NQO1) and gamma-glutamylcysteine synthetase (GCLC), both of which are also targets of Nrf2. As expected, they were up-regulated in HPI cells (Figure 8A). However, Nrf2 itself, and phosphorylated Nrf2 (p-Nrf2), active form of Nrf2, were not increased, whereas Maf G, a member of the Maf family, was increased but slightly. As p-Nrf2 is translocated to nucleus, then we performed immunoblot analysis separately for cytosol and nucleus and found that amount of p-Nrf2 in nucleus was more in HPI cell (Figure 8B), indicting that p-Nrf2 increased in nuclei to transactivate its related genes.

To determine whether the Nrf2/Maf-G-controlled genes were constitutively up-regulated in HPI cell, we explored their expression in the aforementioned CuHPI cells, in which HCV had been eliminated. In spite that HCV proteins were not detected in the CuHPI cell, the Nrf2 target genes were constitutively increased in CuHPI cells regardless of the presence of HCV. Although Nrf2, p-Nrf2 and Maf G did not change much (Figure 8C), p-Nrf2 in the nucleus was increased in the CuHPI cells as observed in HPI cell (Figure 8D). These results indicate that the transactivation of the Nrf2 target genes in HPI cell might be attributed to the constitutive increase of nuclear p-Nrf2.

Knockdown of Nrf2 Reduced Lipid Droplets and HCV

Then, to investigate whether Nrf2 affects lipid accumulation and HCV infection in HPI cell, we performed Nrf2 knockdown with small interfering RNA (siRNA). Knockdown of Nfr2 reduced expression of the target genes, NQO1, GCLC, G6PD and ASNS albeit with less extent in MTHFD2 and PCK2 (Figure 9A) in HPI cell. Importantly, the knockdown reduced HCV proteins, core and NS5A, remarkably. Reduction of HCV was verified at RNA level as well by RT-PCRs for overlapping three portions of HCV genome (Figure 9B). Moreover, fluorescence histochemistry showed that Nrf2 knockdown markedly reduced LDs and HCV infection in HPI cell (Figure 9C). Cellular lipid contents were actually reduced by the knockdown of Nrf2 (Figure 9D). Especially, reduction of triacylglycerol, main component of LD, was greatest. Collectively, these results indicate that Nrf2 and its target genes are intimately involved in the lipid metabolism of HPI cell, especially in LD formation, and persistent infection of HCV.

Discussion

Although cell culture systems for HCV-persistent-infection have been reported, the period of persistency is months [7–9]. Therefore, HPI cell is a *bona fide* HCV-persistently-infected cell line because it has supported HCV for more than two years. Clinically, genotype 1b HCV is more susceptible to chronic hepatitis leading to liver cirrhosis and carcinoma, and thus an infectious strain of genotype 1b has been more required and actually established [20]. However, its infectivity is not so robust as the JFH-1. Therefore, we generated chimeric HCV, TNS2J1, and have used it for transient infection experiments [5] [6]. We started with both JFH-1 and TNS2J1 for a persistent infection system. However, JFH-1-infected cells vanished completely after 3 months, the reason why was unknown.

It was noteworthy that HPI cell has sustained steatosis as observed in chronic hepatitis C for long term. HCV modulates lipid metabolism to promote HCV replication [21,22] and induces steatosis in its transgenic mice [23]. HCV core protein associates with LDs [15,24]. Moreover, LDs are shown to function in the assembly and release of HCV particles dependent on apolipoprotein B expression and VLDL secretion [25–27]. Thus, we speculate the core protein plays a pivotal role in the development of steatosis as 'a viral factor' in HPI cells.

Since HMGCR is known to increase cholesterol and inhibitors of HMGCR, statins, inhibit HCV replication [28], it may be involved also in the persistence of HCV in HPI cells. Recent reports demonstrated that miroRNA-122 (miR-122) regulates cholesterol metabolism by the down-regulation of HMGCR [29] and HCV replication [30], Moreover, deletion of miR-122 results in hepatosteatosis and tumorigenesis in mice [31]. Therefore, investigation of miroRNA including miR122 will be required for HPI cell.

In relation to cholesterol, desmosterol was increased remarkably in HPI cell. Desmosterol is an immediate precursor of cholesterol. This conversion is catalyzed by 24-dehydrocholesterol-reductase (DHCR24). A number of recent researches have shed light on unexpected and new roles of desmosterol and DHCR24 in metabolic diseases including hepatitis C [32]. Another metabolite profiling study also showed increase of desmosterol in the HCV-infected cells and demonstrated that activity of DHCR7, which catalyzes the reaction of desmosterol precursor to desmosterol, was important for HCV replication [33]. We speculate that rather up-regulation of HMGCH, rate-limiting enzyme for cholesterol, and SC5DL might enhance cholesterol synthesis pathway in the HPI cell and that down-regulation (0.6-fold) of DHCR24 might reduce

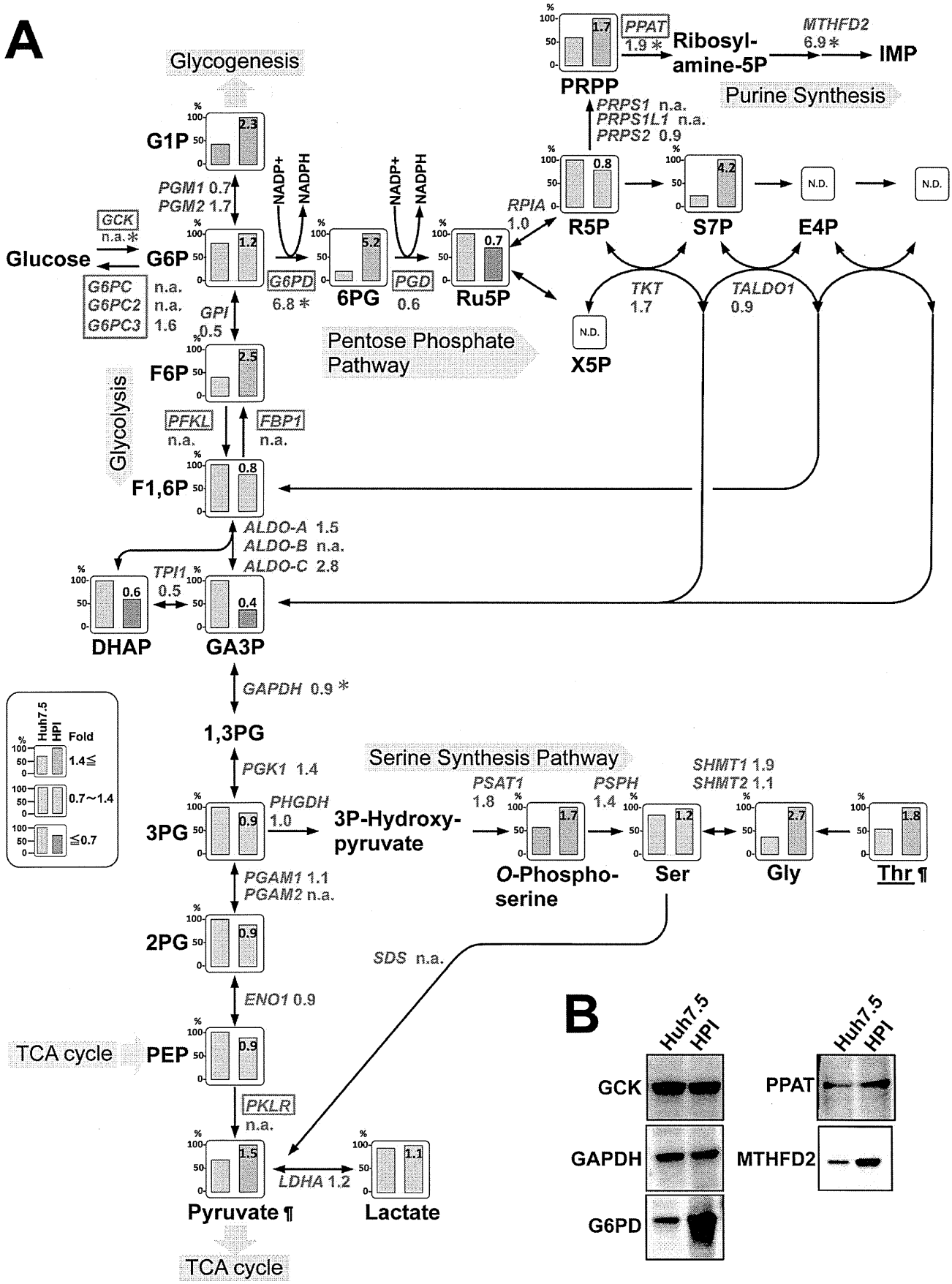
A
Glycogenesis
G1P
PGM1 0.7
PGM2 1.7
GCK
n.a.*
Glucose
G6P
G6PC
G6PC2
G6PC3
n.a.
n.a.
1.6
GPI
0.5
F6P
PFKL
n.a.
FBP1
n.a.
Glycolysis
F1,6P
ALDO-A 1.5
ALDO-B n.a.
ALDO-C 2.8
TPI1
0.5
DHAP
GA3P
GAPDH 0.9 *
1,3PG
PGK1 1.4
PHGDH
1.0
3PG
PGAM1 1.1
PGAM2 n.a.
2PG
ENO1 0.9
PEP
PKLR
n.a.
Pyruvate ¶
LDHA 1.2
Lactate
TCA cycle
TCA cycle
NADP+
NADPH
G6PD
6.8 *
6PG
PGD
0.6
Ru5P
RPIA
1.0
R5P
S7P
E4P
N.D.
TKT
1.7
TALDO1
0.9
X5P
Pentose Phosphate Pathway
PPAT
1.9 *
PRPP
Ribosyl-
amine-5P
MTHFD2
6.9 *
IMP
Purine Synthesis
PRPS1 n.a.
PRPS1L1 n.a.
PRPS2 0.9
Serine Synthesis Pathway
PSAT1
1.8
3P-Hydroxy-
pyruvate
PSPH
1.4
O-Phospho-
serine
Ser
SHMT1 1.9
SHMT2 1.1
Gly
Thr ¶
SDS n.a.
Huh7.5
HPI
Fold
1.4≦
0.7~1.4
≦0.7
B
Huh7.5
HPI
GCK
GAPDH
G6PD
PPAT
MTHFD2

Figure 6. Glycolysis, pentose phosphate pathway, and serine synthetic pathway. (**A**) A metabolic map of glycolysis, the pentose phosphate pathway, and the serine synthetic pathway with gene expression is depicted in the same way as in Figure 4. Underlined: essential amino acid. Abbreviations: G1P, glucose-1-phosphate; G6P, glucose-6-phosphate; F6P, fructose 6-phosphate; F1,6P, fructose 1,6-diphosphate; DHAP, dihydroxyacetone phosphate; GA3P, glyceraldehyde 3-phosphate; 1,3PG, 1,3-Bisphosphoglycerate; 3PG, 3-Phosphoglyceric acid; 2PG, 2-phosphoglycerate; PEP, phosphoenolpyruvate; 6PG, 6-phosphogluconolactone; Ru5P, ribulose 5-phosphate; X5P, xylulose 5-phosphate; R5P, ribose 5-phosphate; S7P, sedoheptulose 7-phosphate; E4P, erythrose 4-phosphate; X5P, xylulose 5-phosphate; PRPP, phosphoribosyl pyrophosphate; IMP, inosine monophosphate; Ser, serine; Gly, glycine; Thr, threonine. Symbols (¶, *, N.D., n.a.) represent the same meaning as in Figure 4A. (**B**) Immunoblot analysis of the selected enzymes. The control was the same beta-actin as in Figure 4B.
doi:10.1371/journal.pone.0094460.g006

the reaction of desmosterol to cholesterol resulting in the accumulation of desmosterol. Feedback inhibition of DHCR24 by lipid accumulation such as cholesterol and fatty acids is possible in HPI cell, although further study will be needed. Collectively, we strongly suggest that desmosterol could be a new biomarker for liver steatosis.

Enrichment of fatty acid pool was demonstrated in HPI cells. We speculate that was because of increase in the synthesis by the up-regulation of ACACA and/or because of decrease in the release by the down-regulation of DGAT1 and MTTP, both of which facilitate VLDL release. It is considered that down-regulation of LIPC and up-regulation of PNPLA3 might be a negative feedback reaction against the excess amount of fatty acid pool, triacylglycerol and LD. Increase of desaturated fatty acids, which have more than 2 double bonds of carbons, were observed in the HPI cell. This could be elucidated mainly by the up-regulation of SCD, an enzyme to catalyze desaturations. Since HCV core alone up-regulates SCD and accumulates NADH resulting in reductive status and enhancement of fatty acid desaturation [34], core protein might be most responsible also in HPI cell. Moreover, ethanol enhances HCV replication through lipid metabolism and elevated NADH/NAD+ [35]. Although NADH level was not elevated in the HPI cell, NADPH was more increased, indicating that NADPH might play a predominant role in the desaturation of fatty acids. Intriguingly, we observed that these cells were rich in 20-carbon fatty acids such as arachidonic acid, which is a precursor of inflammatory mediators, the so-called eicosanoids, and can cause chronic inflammation, inducing inflammatory signals around the cell[36–38].

The Warburg effect is the well-established theory that cancer cells preferentially utilize glycolysis [39]. However, in spite that HPI cells are originated form hepatocellular carcinoma, the TCA cycle was more activated than the glycolysis. Thus we speculate that, contrary to common cancers, hepatic cancer infected with HCV might preferentially utilize the TCA cycle in aerobic condition as previously reported [40]. In fact, hepatic cancers are vascular-rich and prone to demand more oxygen. Interestingly, alternative pathways in the glycolysis were facilitated relating to cancer promotion such as the PPP, purine synthesis pathway and the serine synthetic pathway as described previously [40] [41]. In HPI cells, level of NADPH was high, which might be synthesized not only by G6PD from the PPP and but also ME1 form the TCA cycle. In general, synthesized NADPH is utilized for reductive biosynthesis of cholesterol and fatty acids for LD formation as well as cytoprotection by reduction of reactive oxygen species, as could have occurred in HPI cells.

HPI cells were in a hypermetabolic status producing various metabolites, especially high-energy molecules such as ATP and NADPH, and accumulating energy in the form of LDs. But where did the energy come from? Increased uptake into the cell and/or decreased release from the cell could be thinkable. Cultured hepatoma cell, Huh7.5 or HPI, take in nutrients constantly from outside the cell. We have used culture medium containing 4.5 g/l glucose, which is higher than normal glucose level in human blood (1–2 g/l). Such high glucose concentration might have forced the cells to take up excess amounts of glucose. However, there is an opposite report mentioning that gluconeogenesis is promoted by HCV infection through an HCV NS5A-mediated, FoxO1-dependent signaling pathway [42]. We also noticed up-regulation of PCK2 in HPI cells. Therefore, further study on glucose metabolism will be needed to clarify these issues.

The remarkable elevation of intracellular essential amino acid indicates increased uptake of essential amino acids from the medium, whereas the elevation of non-essential amino acid levels suggests increased in intracellular *de novo* synthesis or both. For uptake of extracellular amino acids, amino acid transporters play an important role [43] and are classified into families of soluble carrier (SLC) (http://www.bioparadigms.org/slc/menu.asp) [44]. Reportedly, glucose and amino acids are increased in tumor cells to meet the increased demand for robust proliferation, for example, by the induction of SLC2A1 and SLC5A1 for glucose [45], and by the induction of SLC7A5 for amino acids [46]. In the present study, the microarray analysis showed that some genes encoding amino acid transport were up-regulated also in HPI cells (Table S4). Of them, up-regulation of SLC1A5, SLC7A1, and SLC7A11 were remarkable, possibly leading to the increase of amino acid intake (Table S4). Notably, SLC7A11, which is a cysteine transporter (xCT), confers resistance against oxidative stress and is related to multiple cancers [47].

Table 2. Intracellular concentration of NAD(P)+ and NAD(P)H.

Metabolite	Huh7.5	HPI	Fold:
	pmol/10^6 cells	pmol/10^6 cells	HPI/Huh7.5
NAD+	752	1500	2.0
NADH	(3.1E-03)	(2.4E-03)	0.8
NADP+	110	132	1.2
NADPH	(6.1E-03)	(9.7E-03)	1.6

Numeral in a parenthesis indicates relative area by the CE-FOFMS.
doi:10.1371/journal.pone.0094460.t002

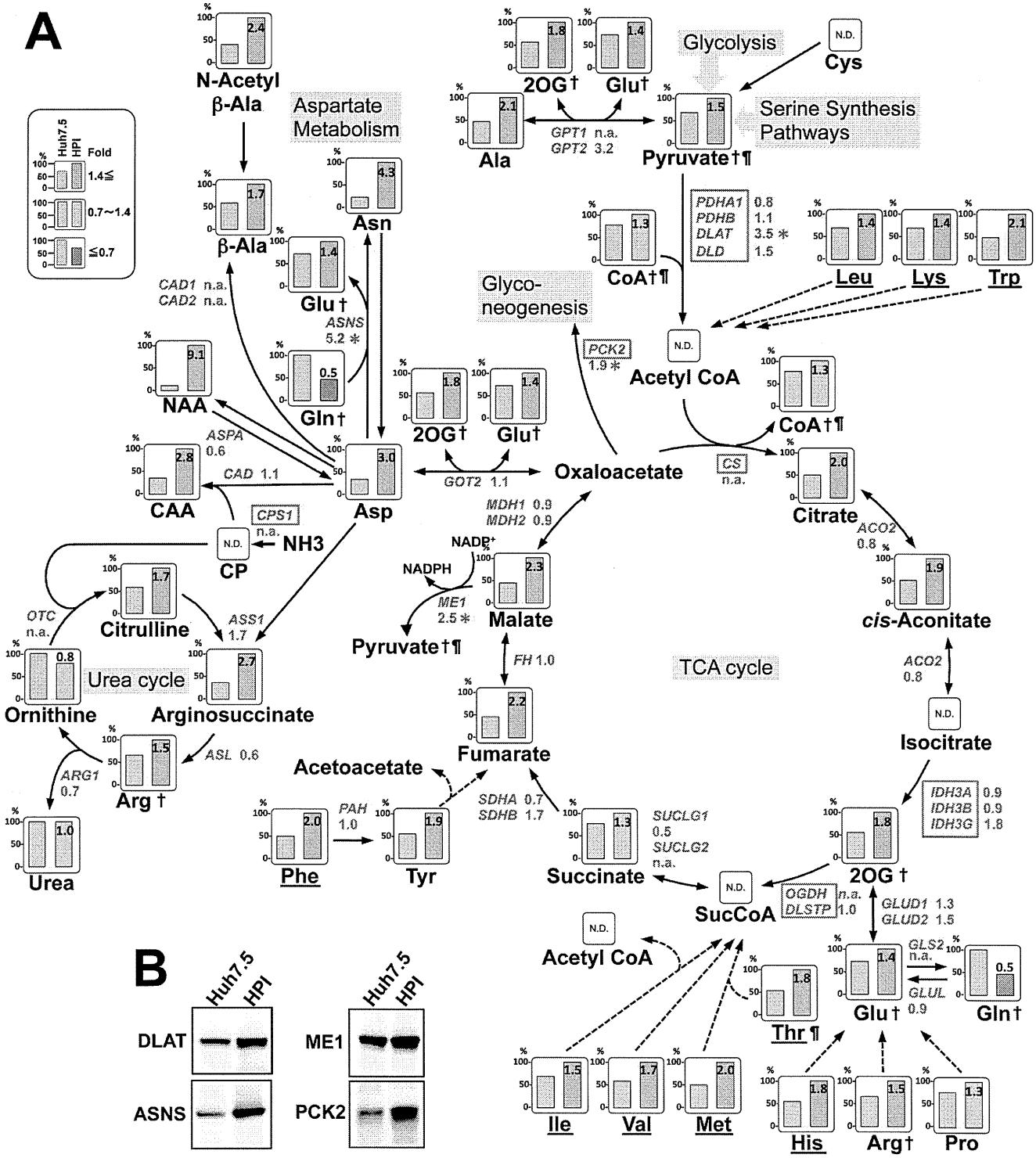

Figure 7. TCA cycle, amino acid metabolism, and the urea cycle. (**A**) A metabolic map of the TCA cycle, amino acid metabolism, and the urea cycle with gene expression is depicted in the same way as in Figure 4. Underlined: essential amino acid. †: Metabolite appearing more than twice in this figure. Abbreviations: Cys, cysteine; Ala, alanine; Glu, glutamate; 2OG, 2-oxoglutarate; Leu, leucine; Lys, lysine; Trp, tryptophan; Gln, glutamine; Pro, proline; Arg, arginine; His, histidine; Met, methionine; Val, valine; Ile, isoleucine; Phe, phenylalanine; Tyr, tyrosine; Asp, aspartate; NAA, N-acetylaspartate; CAA, N-carbamoyl aspartate; CP, carbamoyl phosphate; NH3, ammonia. Symbols (¶, *, N.D., n.a.) represent the same meaning as in Figure 4A. (**B**) Immunoblot analysis of the selected enzymes. The control was the same beta-actin as in Figure 4B.
doi:10.1371/journal.pone.0094460.g007

Present study is the first to demonstrate that the metabolic genes under the control of Nrf2, such as G6PD, MTHFD2, ASNS, ME1 and PCK2, were involved in persistent infection with HCV, although some reports showed Nrf2 induces just antioxidant and

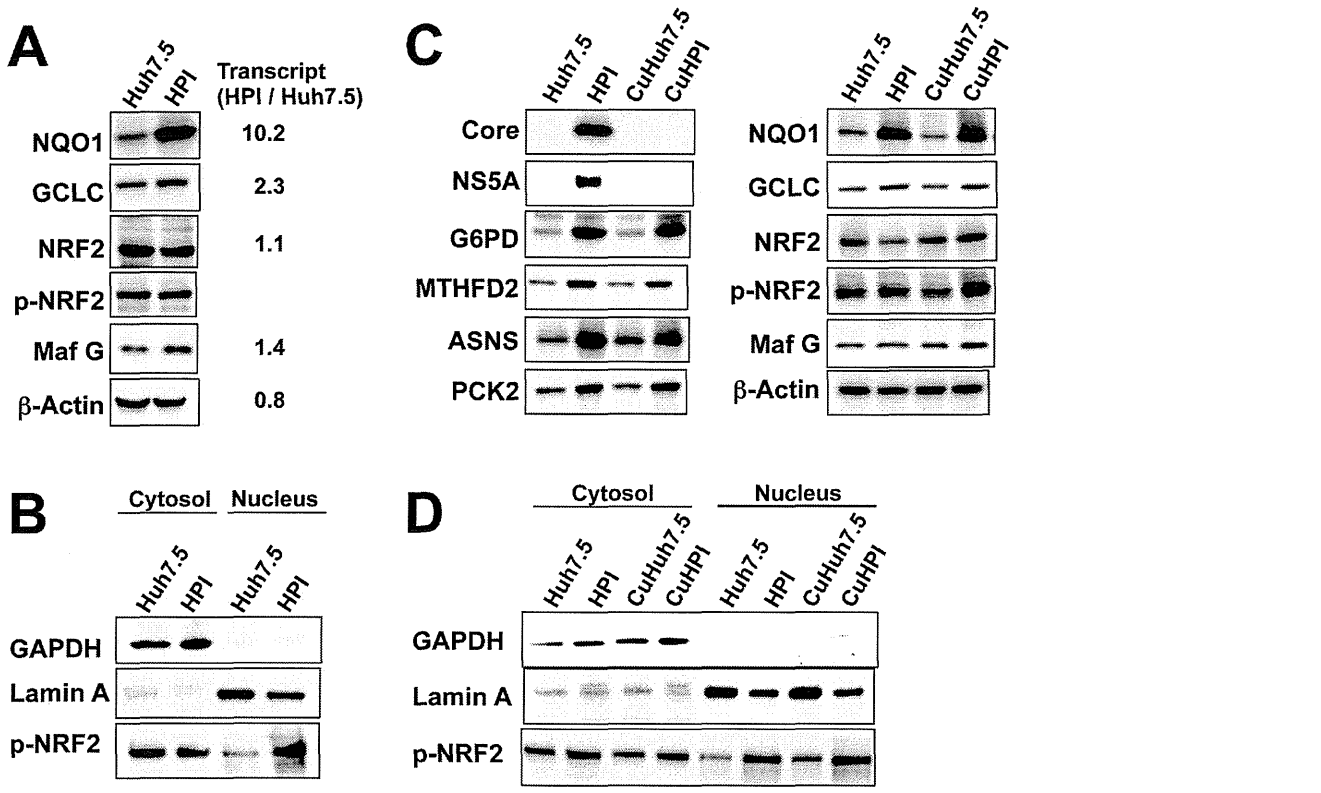

Figure 8. Expression of Nrf2, Maf G, and Nrf2-targert genes. (**A**) Immunoblot analyses of the proteins related to antioxidation and detoxification, Nrf2, phosphorylated Nrf2 (p-Nrf2), and Maf G for Huh7.5 and HPI cells. Fold expression of transcript (HPI/Huh7.5) in corresponding genes was shown in the right according to the expression array data. (**B**) Immunoblot analysis of p-Nrf2 in cytosol and nucleus fractions from the cells used in (A). GAPDH and Lamin A were used as a marker protein for cytosol and nucleus, respectively. (**C**) Immunoblot analyses of the HCV core and NS5A proteins, Nrf2-trarget genes, Nrf2, p-Nrf2 and Maf G for Huh7.5 and HPI cells, CuHuh7.5 cells (Huh7.5 cells simply treated with cyclosporine) and CuHPI cells (HPI cells, from which HCV was eliminated with cyclosporine). (**D**) Immunoblot analysis of p-Nrf2 in their cytosol and nucleus fractions from the cells used in (C).
doi:10.1371/journal.pone.0094460.g008

detoxifying genes in HCV-infected cells [48] [49]. According to the immunoblot analyses, Maf G was increased in HPI cell, but the extent was slight. Thus we suggest that translocation of p-Nrf2, active form of Nrf2, might play a more important role in the expression of the genes, which contribute to anti-apoptosis and HCV persistence. Actually, P-Nrf2 was constitutively increased in the nucleus of HPI cell and the genes under its control were also constitutively activated. Although precise mechanism is unclear, it is speculated that some genetic or epigenetic alterations could have occurred during the long-term culture and the clonal selections affecting the Nrf2/Maf system.

Drastic reduction of LDs and lipid contents by the Nrf2 knockdown indicates that steatosis is dependent of Nrf2 in HPI cell. Additionally, we demonstrated that knockdown of Nrf2 reduced HCV infection. Reduction of its target gene expression by the Nrf2 knockdown varied, suggesting that extent of transactivation by Nrf2 and protein stability is dependent on an individual gene. Since HCV infectious cycle is closely related to lipid metabolism and LDs [15,50], reduction of HCV by the Nrf2 knockdown might have been caused via impairment of lipid metabolism. We need to know which target gene(s) are more responsible for HCV infection and lipid metabolism.

Emerging anti-HCV drugs will bring about further improvement in sustained virological response in HCV patients. Recent study showed the risk of HCC remains even after sustained virological response [51] [52]. Genetic or epigenetic alterations that had occurred in the hepatocytes in the HCV patients for long-term chronic infection may increase HCC risk. Nrf2 and/or its target gene might be involved in candidates of such genetic alteration, because Nrf2 is activated in many cancers and would favor cell growth arrest of cancers [53,54] Thus, genetic experiments like ultra-deep sequencing will be needed in search of such alterations in both HPI cell and clinical HCC. Moreover, Nrf2 inhibitor could be anti-HCV drug as well as anti-HCC drug, although detrimental effects on cytoprotection and detoxification must be considered.

In conclusion, we established a *bona fide* HCV-persistently-infected cell line supporting HCV for more than two years bearing prominent steatosis. Integrated analysis by metabolomics and expression arrays revealed that this cell line was in a hypermetabolic status facilitating lipid synthesis, PPP, purine synthesis, serine synthesis and TCA cycle. Transcription factor complex Nrf2/Maf-G may be involved in such a metabolic alteration. This cell line is a potent research tool not only for persistent HCV infection, but also for hepatic metabolic, connecting infection, inflammation and carcinogenesis.

Materials and Methods

Cell Culture, RNA Transfection and Limiting Dilution

Huh 7.5 cells were cultured in high-glucose DMEM (Life technology) supplemented with 10% fetal calf serum. The cultured

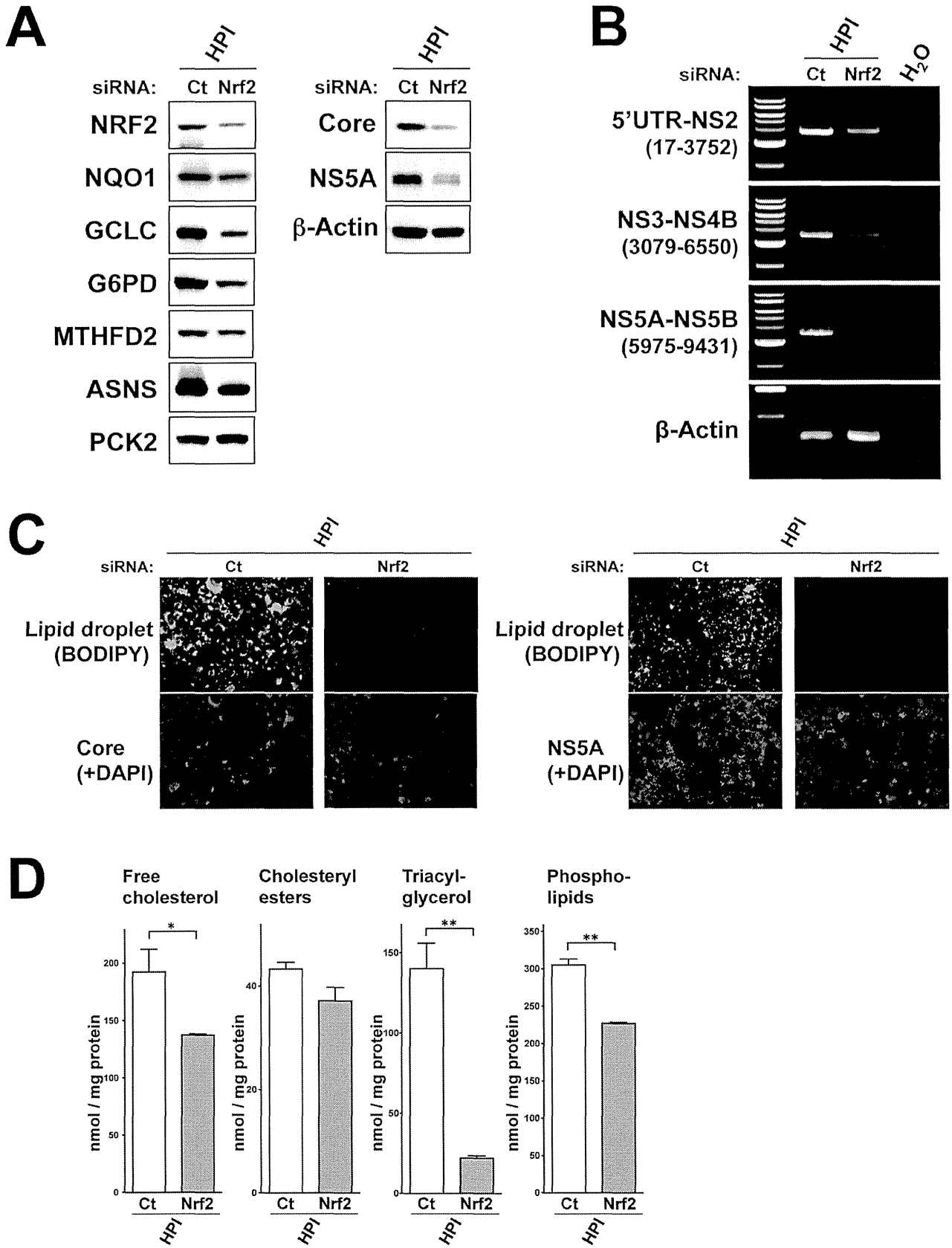

Figure 9. Knockdown of Nrf2 reduced lipid droplets and HCV in HPI cell. For knockdown of Nrf2, HPI cells were transfected with siRNA for Nrf2 or negative control siRNA (Ct) three times and were analyzed 2 days after the last transfection. (**A**) Immunoblot analysis of the protein for Nrf2, Nrf2-target genes and HCV (core and NS5A) was performed. (**B**) RT-PCRs were performed for three parts of HCV (5'UTR-NS2, NS3-NS4B and NS5A-

NS5B) covering the full genome of HCV. Number in parenthesis indicates HCV nucleotide position amplified by RT-PCR. The most left lane of each panel represents size maker (2, 3, 4, 5, 6, 8 and 10 kb) for HCV and that for β-actin (0.2, 0.3 and 0.4 kb). (**C**) Fluorescence staining for LDs and simultaneous immunofluorescence staining for HCV core and NS5A proteins (four left panels and four right panels, respectively) were performed. Nuclei were counterstained with DAPI. (**D**) Intracellular lipid contents were determined in triplicate. Values were corrected by the protein concentration and statistically evaluated by Student's *t*-test indicating a significance of $P<0.05$ (*) and $P<0.01$ (**).
doi:10.1371/journal.pone.0094460.g009

cells was transfected with synthesized RNA of TNS2J1 as described previously [55]. Then, the cells were serially passaged in 1:3 or 1:4 splits. Concentrations of the HCV core protein in the medium were determined by using an ELISA kit (Ortho Diagnostic, Japan). Limiting dilution was performed by seeding the cultured cells on a 96-well-plate containing 0.5 cells/well.

Preparation of Cell Cured of HCV

HCV-persistently-infected cells was cultured with the medium containing 1 μg/ml cyclosporine A (Sigma) for 3 weeks to eliminate HCV and subjected to limiting dilution to isolate cell cured of HCV. No production of HCV was confirmed by the ELISA kit for core protein in medium and by immunofluorescence staining for intracellular HCV proteins. The cured cell was designated CuHPI.

Virus Infection, Titration, and Sedimentation Analysis

HCV infection was performed by inoculation of culture medium containing HCVcc. Determination of HCV infectivity (FFU) and sedimentation analysis for HCVcc were performed as mentioned previously [56].

Immunofluorescence and Cytochemical Staining

For immunofluorescence staining, cells were seeded on a chamber slide. After 2 days, they were fixed with 4% paraformaldehyde, permeabilized with 0.1% Triton X-100 solution, and blocked with 5% BSA. They were incubated with primary antibodies (1 h) and then with secondary antibody (1 h). BODIPY and DAPI were used for cytochemical staining for LDs and nucleoli, respectively. Oil Red O staining (Muto pure chemicals, Japan) and crystal violet staining (Merck) was used for detection of lipid droplet and living cells, respectively.

Extraction of Cytosol and Nucleus Fractions

Extraction of cytosol and nucleus fractions from cultured cell was conducted by using NE-PR nuclear and cytoplasmic extraction reagents (Thermo) according to the manufacture's protocol.

Immunoblot Analysis

For immunoblot analysis, cultured cells were harvested in lysis buffer (Pierce). After the addition of an equal volume of 2X Laemmli sample buffer (Biorad) with 5% β-mercaptoethanol, they were heat denatured (95°C, 5 min), sonicated (10 min), and then subjected to SDS-PAGE. Proteins were transferred to a PVDV membrane, Immobilon-P (Millipore), and were blocked with 5% milk powder and subsequently incubated with primary antibody. Then after incubation with horseradish peroxidase-conjugated secondary antibody for 1 h, the proteins were visualized with the ECL Prime (Amersham).

Primary and Secondary Antibodies for Immunofluorescence Stain and Immunoblot Analysis

Primary antibodies were for HCV proteins: core (Institute of immunology), NS5A (Antiprot), NS3 (Antiprot), NS5A (Virogen), and NS5B (Antiprot), beta-Actin (Abcam), ACYL (Cell signaling), HMGCR (Atlas antibodies), DHCR7 (Abcam), ACACA (Santa Cruz), ELOVL5 (Novusbio), GPAM (Abcam), MTTP (Abcam), PNPLA3 (Abcam), GCK (Santa Cruz), GAPDH (Abcam), G6PD (Santa Cruz), PPAT (Proteintech), MTHFD2 (Proteintech), PSAT1 (Santa Cruz), SHMT1 (Abcam), G6PC3 (Santa Cruz), DLAT (Santa Cruz), IDH3G (Santa Cruz), ASNS (Santa Cruz), ME1 (Abcam), PCK2 (Abcam), GPT2 (Santa Cruz), NQO1 (Proteintech), GCLC (Abnova), Nrf2 (Santa Cruz), phosphorylated-Nrf2 (Abcam), Maf-G (Abcam), Lamin A (Santa Cruz). HRP-labeled secondary antibodies were used against mouse IgG, rabbit IgG, and goat IgG (Amersham) dependent on the primary antibodies for immunoblot. Alexa-fluor-568-labeled goat anti-mouse secondary antibody (Invitrogen) was used for immunofluorescence.

Quantification of Cellular Lipid Contents

Cells were suspended in PBS and disrupted by sonication. Protein concentrations of whole cell homogenates were determined using a BCA protein assay kit (Pierce). Total lipids were extracted from the homogenate according to the Bligh and Dyer method. Details of Quantification of each Lipid Contents are described in the Supporting Methods. Three ml of chloroform/methanol = 1/2 (v/v) was added to 0.8 ml of the homogenate containing 250–500 μg protein to a give one phase. After 1 ml each of chloroform and PBS were added, lower chloroform phase containing lipids was separated by centrifugation. The entire lower phase was dried up under nitrogen gas and dissolved in a small volume of chloroform/methanol = 1/2 (v/v). The lipid extract was spotted on a silica gel G60 plate (Merck) and then separated by thin-layer chromatography using hexane/diethyl ether/acetic acid = 70/30/1 (v/v) as a solvent system. Free and esterified cholesterol, triacylglycerol, and phospholipids were visualized with iodine vapors and marked. Each lipid was removed from the silica gel by scraping the appropriate area from the thin-layer plate and extracted by Bligh and Dyer method.

1) Determination of Free and Esterified Cholesterol Contents

Free and esterified cholesterol extracted from silica gel were dried up and dissolved in 0.5 ml of acetone. Cholesterol content in the acetone extract was fluorometrically determined using enzymatic reactions as described. Briefly, an aliquot (5 μl) of the extract or cholesterol standard (up to 1 nmol) was transferred to a well of a 96-well black plate (Labsystems) containing 50 μl/well of reaction buffer (0.1 M potassium phosphate pH 7.4, 50 mM NaCl, 5 mM cholic acid, 0.1% Triton X-100). The reactions were initiated by adding 50 μl/well of the reaction buffer containing 300 μM Ampliflu red (Sigma), 2 U/ml cholesterol oxidase, 2 U/ml horseradish peroxidase, and 0.2 U/ml cholesterol esterase (for quantification of esterified cholesterol) and allowed to proceed for 30 min at 37°C. Fluorescence intensities were measured using a multi-well plate reader (FLUOstar Optima, BMG Labtech) equipped with a filter set for excitation and emission at 544 and 590 nm, respectively.

2) Determination of Triacylglycerol Content

Triacylglycerol extracted from silica gel was dried up and then dissolved in 0.2 ml of 2-propanol. An aliquot (10 µl) was assayed for triacylglycerol content by using Triglyceride (INT) reagent (Sigma diagnostics) with cholesteryl oleate as a standard according to the manufacturer's protocol.

3) Determination of Phospholipid Content

Total phospholipids extracted from silica gel were dried up and then dissolved in 0.5 ml of chloroform/methanol = 1/2 mixture (v/v). An aliquot (100 µl) was dried up and then assayed for phosphate content as described (Lipids, 1, 85, 1966). Briefly, the dried phospholipids were digested with 140 µl of 70% perchloric acid at 180°C for 1 hr to release inorganic phosphates. The digested fraction was mixed with 800 µl of H_2O/1.25% ammonium molybdate/10% ascorbic acid = 5/2/1 and then heated at 100°C for 5 min. Absorbance of the phosphate-molybdate complex at 820 nm was measured using a spectrophotometer (Shimadzu UV-1700). The amount of inorganic phosphate was determined using KH_2PO_4 as a standard.

Expression Array

The Huh7.5 and HPI cells (4×10^6 each) were plated onto 10-cm diameter dishes and cultured for 2 days. Total RNAs from these cells (approximately 80% confluence) were prepared using an RNeasy extraction kit (QIAGEN). For expression array, cDNA microarray analysis was performed with a Human Oligo Chip 25K (Toray, Japan) and analyzed by a 3D-Gene scanner 3000 (Toray). Result of the microarray was deposited in Gene Expression Omnibus (accession number: GSE52321).

CE-TOFMS Measurement

A dish of cultured cells (10^6 cells/sample) was used for the extraction of intracellular metabolites. The culture medium was aspirated from the dish and cells were washed twice by 5% mannitol solution (10 ml first and then 2 ml). The cells were then treated with 800 µl of methanol and left to rest for 30 s in order to inactivate enzymes. Next, the cell extract was treated with 550 µl of Milli-Q water containing internal standards (H3304-1002) and left to rest for another 30 s. The extract was obtained and centrifuged at 2,300×*g* and 4°C for 5 min, and then 800 µl of the upper aqueous layer was centrifugally filtered through a Millipore 5-kDa cutoff filter at 9,100×*g* and 4°C for 120 min to remove proteins. The filtrate was centrifugally concentrated and re-suspended in 50 µl of Milli-Q water for CE-MS analysis (Human metabolome technologies, Japan).

LC-TOFMS Measurement

Cell cultures were prepared and washed as per above. The cells were then treated with 1,300 µl of ethanol containing an internal standard (H3304-1002) in order to inactivate enzymes. The cells were scraped from the plate, and 1,000 µl of cell lysate was mixed with 1,000 µl of Milli-Q water by ultrasonication on ice for 5 min. After the mixture solution was centrifuged at 2,300×*g* and 4°C for 5 min, the supernatant was desiccated and then dissolved with 100 µl of isopropanol/Milli-Q water for LC-MS analysis (Human metabolome technologies).

Knockdown of Nrf2 Gene

Cultured cells were transfected with Stealth siRNA (5′-UCACUUUGCAAAGCUUUCAACCAAA-3′, 5′-UUUGGUUGAAAGCUUUGCAAAGUGA-3′, Life technology) for knockdown of Nrf2 or Negative Control Duplexes (Life technology) as a negative control by using Lipofectamine RNAiMax reagent (Life technology).

RT-PCR

RT-PCRs were performed to amplify three parts of HCV genome; 5′UTR-NS2, NS3-NS4B and NS5A-NS5B, with primers listed on Table S5. Reverse transcription was done at 55°C for an hour with Superscript III (Life technology). Polymerase chain reaction was done with KOD plus (Toyobo, Japan) by 18 cycles of a reaction (98°C denaturing for 10 seconds, 60°C annealing for 30 seconds and 68°C extension for 3.5 minutes).

Supporting Information

Figure S1 Long-term existence of HCV in HPI cells. (A) RT-PCR for the 5′UTR-NS2 region and the NS3-NS5B region of HCV were performed using total RNA from Huh7.5 cells, TNS2J1-infected Huh7.5 cells (lytic phase), and HPI cells (passages 8 and 176). **(B)** Immunoblot analyses of the HCV core, NS3, NS5A, and NS5B were performed using cellular proteins from the same cells as in (A).
(TIF)

Figure S2 Characterization of HCVcc from HPI cells. (A) Sedimentation analysis of HCVcc from HPI cells. Left and right y-axes represent HCV core protein concentration (filled circles) and infectivity (filled squares) forming peaks at buoyant densities of 1.117 mg/ml and 1.108 mg/ml, respectively. **(B)** Clonal sequencing of the RT-PCR products (the 5′UTR-NS2 and NS2-NS5B regions) from HCVcc. Deduced amino acid sequences from three clones were compared with the original TNS2J1 sequence, indicating consensus and non-consensus alterations shown by black and gray vertical lines, respectively. Amino acid number corresponds to that of TNS2J1. **(C)** Naïve Huh7.5 cells were inoculated with the culture medium from HPI cells or mock. At day 2 after inoculation, immunofluorescence staining for HCV NS5A protein was performed (the most left upper and lower panels). From this point, every time the mock-transfected cells became confluent, both transfected cell cultures were split (1:4) into two wells of a 6-well plate simultaneously. One well was used for maintaining the cell culture whereas the other was used for crystal violet staining (living cell stain) after the transfection (three upper right and three lower right panels). P-numbers in parentheses represent the passage numbers after transfection. **(D)** A cured cell clone, CuHPI, was inoculated with the supernatant from the cultured HPI cells at a MOI of 0.02 FFU/cell and maintained monitoring HCV core protein in the medium and checking intracellular HCV 5A protein by immunocytochemistry.
(TIF)

Figure S3 Enlarged images of lipid droplets and colocalizing HCV proteins. The merged images of confocal laser scanning microscopy for the HPI cells at passage 8 (middle panels of 4th and 7th from the left in Figure 3A) were enlarged to show colocalization of LDs with HCV core (left) and NS5A (right).
(TIF)

Table S1 Intracellular metabolites detected by LC-TOFMS.
(XLSX)

Table S2 Intracellular metabolites detected by CE-TOFMS.
(XLSX)

Table S3 Expression array data of genes encoding enzymes in metabolomics profiling.
(XLSX)

Table S4 Expression of genes coding an amino acid transporter. (XLSX)

Table S5 Primer List for RT-PCR. (XLSX)

Acknowledgments

We thank Dr. Charles M. Rice, Rockefeller University, for providing Huh7.5 cell, Drs. Toshiaki Teratani, Takahiro Suzuki, and Kengo Tomita, Keio University, for their technical assistance, Ms. Kyoko Watanabe and Ms. Tomoko Osumi, Keio University, for experiment preparation and Dr. Kunitada Shimotohno, National Center for Global Health and Medicine, for scientific advice.

Author Contributions

Conceived and designed the experiments: K. Sugiyama TH HS TK. Performed the experiments: K. Sugiyama NS YM PC SU YS K. Saito. Analyzed the data: K. Sugiyama HE NN YI YW NT HM YY. Contributed reagents/materials/analysis tools: MF TW HT. Wrote the paper: K. Sugiyama.

References

1. Liang TJ, Jeffers LJ, Reddy KR, De Medina M, Parker IT, et al. (1993) Viral pathogenesis of hepatocellular carcinoma in the United States. Hepatology 18: 1326–1333.
2. Hijikata M, Kato N, Ootsuyama Y, Nakagawa M, Shimotohno K (1991) Gene mapping of the putative structural region of the hepatitis C virus genome by in vitro processing analysis. Proceedings of the National Academy of Sciences of the United States of America 88: 5547–5551.
3. Hijikata M, Mizushima H, Tanji Y, Komoda Y, Hirowatari Y, et al. (1993) Proteolytic processing and membrane association of putative nonstructural proteins of hepatitis C virus. Proc Natl Acad Sci U S A 90: 10773–10777.
4. Wakita T, Pietschmann T, Kato T, Date T, Miyamoto M, et al. (2005) Production of infectious hepatitis C virus in tissue culture from a cloned viral genome. Nat Med 11: 791–796.
5. Sugiyama K, Suzuki K, Nakazawa T, Funami K, Hishiki T, et al. (2009) Genetic analysis of hepatitis C virus with defective genome and its infectivity in vitro. J Virol 83: 6922–6928.
6. Nishitsuji H, Funami K, Shimizu Y, Ujino S, Sugiyama K, et al. (2013) Hepatitis C virus infection induces inflammatory cytokines and chemokines mediated by the cross talk between hepatocytes and stellate cells. J Virol 87: 8169–8178.
7. Ploss A, Khetani SR, Jones CT, Syder AJ, Trehan K, et al. (2010) Persistent hepatitis C virus infection in microscale primary human hepatocyte cultures. Proc Natl Acad Sci U S A 107: 3141–3145.
8. Silberstein E, Mihalik K, Ulitzky L, Plant EP, Puig M, et al. (2010) Persistent growth of a human plasma-derived hepatitis C virus genotype 1b isolate in cell culture. PLoS Pathog 6: e1000910.
9. Bauhofer O, Ruggieri A, Schmid B, Schirmacher P, Bartenschlager R (2012) Persistence of HCV in Quiescent Hepatic Cells Under Conditions of an Interferon-Induced Antiviral Response. Gastroenterology 143: 429–438.e428.
10. Goodman ZD, Ishak KG (1995) Histopathology of hepatitis C virus infection. Semin Liver Dis 15: 70–81.
11. Mitsuishi Y, Taguchi K, Kawatani Y, Shibata T, Nukiwa T, et al. (2012) Nrf2 redirects glucose and glutamine into anabolic pathways in metabolic reprogramming. Cancer Cell 22: 66–79.
12. Moi P, Chan K, Asunis I, Cao A, Kan YW (1994) Isolation of NF-E2-related factor 2 (Nrf2), a NF-E2-like basic leucine zipper transcriptional activator that binds to the tandem NF-E2/AP1 repeat of the beta-globin locus control region. Proc Natl Acad Sci U S A 91: 9926–9930.
13. Itoh K, Chiba T, Takahashi S, Ishii T, Igarashi K, et al. (1997) An Nrf2/small Maf heterodimer mediates the induction of phase II detoxifying enzyme genes through antioxidant response elements. Biochem Biophys Res Commun 236: 313–322.
14. Uruno A, Motohashi H (2011) The Keap1-Nrf2 system as an in vivo sensor for electrophiles. Nitric Oxide 25: 153–160.
15. Miyanari Y, Atsuzawa K, Usuda N, Watashi K, Hishiki T, et al. (2007) The lipid droplet is an important organelle for hepatitis C virus production. Nat Cell Biol 9: 1089–1097.
16. Shi ST, Lee KJ, Aizaki H, Hwang SB, Lai MM (2003) Hepatitis C virus RNA replication occurs on a detergent-resistant membrane that cofractionates with caveolin-2. J Virol 77: 4160–4168.
17. Aizaki H, Lee KJ, Sung VM, Ishiko H, Lai MM (2004) Characterization of the hepatitis C virus RNA replication complex associated with lipid rafts. Virology 324: 450–461.
18. Yamazaki T, Sasaki E, Kakinuma C, Yano T, Miura S, et al. (2005) Increased very low density lipoprotein secretion and gonadal fat mass in mice overexpressing liver DGAT1. J Biol Chem 280: 21506–21514.
19. Partin JS, Partin JC, Schubert WK, McAdams AJ (1974) Liver ultrastructure in abetalipoproteinemia: Evolution of micronodular cirrhosis. Gastroenterology 67: 107–118.
20. Date T, Morikawa K, Tanaka Y, Tanaka-Kaneko K, Sata T, et al. (2012) Replication and infectivity of a novel genotype 1b hepatitis C virus clone. Microbiol Immunol 56: 308–317.
21. Kapadia SB, Chisari FV (2005) Hepatitis C virus RNA replication is regulated by host geranylgeranylation and fatty acids. Proc Natl Acad Sci U S A 102: 2561–2566.
22. Hirata Y, Ikeda K, Sudoh M, Tokunaga Y, Suzuki A, et al. (2012) Self-enhancement of hepatitis C virus replication by promotion of specific sphingolipid biosynthesis. PLoS Pathog 8: e1002860.
23. Moriya K, Fujie H, Shintani Y, Yotsuyanagi H, Tsutsumi T, et al. (1998) The core protein of hepatitis C virus induces hepatocellular carcinoma in transgenic mice. Nat Med 4: 1065–1067.
24. Barba G, Harper F, Harada T, Kohara M, Goulinet S, et al. (1997) Hepatitis C virus core protein shows a cytoplasmic localization and associates to cellular lipid storage droplets. Proc Natl Acad Sci U S A 94: 1200–1205.
25. Huang H, Sun F, Owen DM, Li W, Chen Y, et al. (2007) Hepatitis C virus production by human hepatocytes dependent on assembly and secretion of very low-density lipoproteins. Proc Natl Acad Sci U S A 104: 5848–5853.
26. Gastaminza P, Cheng G, Wieland S, Zhong J, Liao W, et al. (2008) Cellular determinants of hepatitis C virus assembly, maturation, degradation, and secretion. J Virol 82: 2120–2129.
27. Icard V, Diaz O, Scholtes C, Perrin-Cocon L, Ramiere C, et al. (2009) Secretion of hepatitis C virus envelope glycoproteins depends on assembly of apolipoprotein B positive lipoproteins. PLoS ONE 4: e4233.
28. Ikeda M, Abe K, Yamada M, Dansako H, Naka K, et al. (2006) Different anti-HCV profiles of statins and their potential for combination therapy with interferon. Hepatology 44: 117–125.
29. Esau C, Davis S, Murray SF, Yu XX, Pandey SK, et al. (2006) miR-122 regulation of lipid metabolism revealed by in vivo antisense targeting. Cell Metabolism 3: 87–98.
30. Jopling CL, Yi M, Lancaster AM, Lemon SM, Sarnow P (2005) Modulation of Hepatitis C Virus RNA Abundance by a Liver-Specific MicroRNA. Science 309: 1577–1581.
31. Hsu SH, Wang B, Kota J, Yu J, Costinean S, et al. (2012) Essential metabolic, anti-inflammatory, and anti-tumorigenic functions of miR-122 in liver. J Clin Invest 122: 2871–2883.
32. Zerenturk EJ, Sharpe LJ, Ikonen E, Brown AJ (2013) Desmosterol and DHCR24: Unexpected new directions for a terminal step in cholesterol synthesis. Progress in Lipid Research 52: 666–680.
33. Rodgers MA, Villareal VA, Schaefer EA, Peng LF, Corey KE, et al. (2012) Lipid metabolite profiling identifies desmosterol metabolism as a new antiviral target for hepatitis C virus. J Am Chem Soc 134: 6896–6899.
34. Miyoshi H, Moriya K, Tsutsumi T, Shinzawa S, Fujie H, et al. (2011) Pathogenesis of lipid metabolism disorder in hepatitis C: polyunsaturated fatty acids counteract lipid alterations induced by the core protein. J Hepatol 54: 432–438.
35. Seronello S, Ito C, Wakita T, Choi J (2010) Ethanol enhances hepatitis C virus replication through lipid metabolism and elevated NADH/NAD+. J Biol Chem 285: 845–854.
36. Lee JL, Mukhtar H, Bickers DR, Kopelovich L, Athar M (2003) Cyclooxygenases in the skin: pharmacological and toxicological implications. Toxicol Appl Pharmacol 192: 294–306.
37. Ziboh VA, Miller CC, Cho Y (2000) Metabolism of polyunsaturated fatty acids by skin epidermal enzymes: generation of antiinflammatory and antiproliferative metabolites. Am J Clin Nutr 71: 361S–366S.
38. Glass CK, Olefsky JM (2012) Inflammation and lipid signaling in the etiology of insulin resistance. Cell Metab 15: 635–645.
39. Warburg O (1956) On the origin of cancer cells. Science 123: 309–314.
40. Mitsuishi Y Fau - Motohashi H, Motohashi H Fau - Yamamoto M, Yamamoto M (2012) The Keap1-Nrf2 system in cancers: stress response and anabolic metabolism.
41. Maddocks OD, Berkers CR, Mason SM, Zheng L, Blyth K, et al. (2013) Serine starvation induces stress and p53-dependent metabolic remodelling in cancer cells. Nature 493: 542–546.
42. Deng L, Shoji I, Ogawa W, Kaneda S, Soga T, et al. (2011) Hepatitis C virus infection promotes hepatic gluconeogenesis through an NS5A-mediated, FoxO1-dependent pathway. J Virol 85: 8556–8568.
43. Masson J, Sagne C, Hamon M, El Mestikawy S (1999) Neurotransmitter transporters in the central nervous system. Pharmacol Rev 51: 439–464.
44. Hediger MA, Romero MF, Peng JB, Rolfs A, Takanaga H, et al. (2004) The ABCs of solute carriers: physiological, pathological and therapeutic implications of human membrane transport proteinsIntroduction. Pflugers Arch 447: 465–468.
45. Ganapathy V, Thangaraju M, Prasad PD (2009) Nutrient transporters in cancer: relevance to Warburg hypothesis and beyond. Pharmacol Ther 121: 29–40.
46. Fuchs BC, Bode BP (2005) Amino acid transporters ASCT2 and LAT1 in cancer: partners in crime? Semin Cancer Biol 15: 254–266.

47. Lo M, Wang YZ, Gout PW (2008) The x(c)- cystine/glutamate antiporter: a potential target for therapy of cancer and other diseases. J Cell Physiol 215: 593–602.
48. Ivanov AV, Smirnova OA, Ivanova ON, Masalova OV, Kochetkov SN, et al. (2011) Hepatitis C Virus Proteins Activate NRF2/ARE Pathway by Distinct ROS-Dependent and Independent Mechanisms in HUH7 Cells. PLoS ONE 6: e24957.
49. Carvajal-Yepes M, Himmelsbach K, Schaedler S, Ploen D, Krause J, et al. (2011) Hepatitis C virus impairs the induction of cytoprotective Nrf2 target genes by delocalization of small Maf proteins. J Biol Chem 286: 8941–8951.
50. Ogawa K, Hishiki T, Shimizu Y, Funami K, Sugiyama K, et al. (2009) Hepatitis C virus utilizes lipid droplet for production of infectious virus. Proc Jpn Acad Ser B Phys Biol Sci 85: 217–228.
51. Aleman S, Rahbin N, Weiland O, Davidsdottir L, Hedenstierna M, et al. (2013) A risk for hepatocellular carcinoma persists long-term after sustained virologic response in patients with hepatitis C-associated liver cirrhosis. Clin Infect Dis 57: 230–236.
52. Putte DEFvd, Makris M, Fischer K, Yee TT, Kirk L, et al. (2013) Long-term follow-up of hepatitis C infection in a large cohort of patients with inherited bleeding disorders. Journal of Hepatology.
53. Jaramillo MC, Zhang DD (2013) The emerging role of the Nrf2-Keap1 signaling pathway in cancer. Genes Dev 27: 2179–2191.
54. Gañán-Gómez I, Wei Y, Yang H, Boyano-Adánez MC, García-Manero G (2013) Oncogenic functions of the transcription factor Nrf2. Free Radical Biology and Medicine.
55. Kato N, Sugiyama K, Namba K, Dansako H, Nakamura T, et al. (2003) Establishment of a hepatitis C virus subgenomic replicon derived from human hepatocytes infected in vitro. Biochem Biophys Res Commun 306: 756–766.
56. Hishiki T, Shimizu Y, Tobita R, Sugiyama K, Ogawa K, et al. (2010) Infectivity of hepatitis C virus is influenced by association with apolipoprotein E isoforms. J Virol 84: 12048–12057.

Hepatology Research

Hepatology Research 2014; 44: 31–42 doi: 10.1111/hepr.12147

Review Article

Alterations of epigenetics and microRNA in hepatocellular carcinoma

Yoshimasa Saito,[1,2] Sana Hibino[1] and Hidetsugu Saito[1,2]

[1]Division of Pharmacotherapeutics, Faculty of Pharmacy, and [2]Division of Gastroenterology and Hepatology, Department of Internal Medicine, School of Medicine, Keio University, Tokyo, Japan

Studies have shown that alterations of epigenetics and microRNA (miRNA) play critical roles in the initiation and progression of hepatocellular carcinoma (HCC). Epigenetic silencing of tumor suppressor genes in HCC is generally mediated by DNA hypermethylation of CpG island promoters and histone modifications such as histone deacetylation, methylation of histone H3 lysine 9 (H3K9) and tri-methylation of H3K27. Chromatin-modifying drugs such as DNA methylation inhibitors and histone deacetylase inhibitors have shown clinical promise for cancer therapy. miRNA are small non-coding RNA that regulate expression of various target genes. Specific miRNA are aberrantly expressed and play roles as tumor suppressors or oncogenes during hepatocarcinogenesis. We and other groups have demonstrated that important tumor suppressor miRNA are silenced by epigenetic alterations, resulting in activation of target oncogenes in human malignancies including HCC. Restoring the expression of tumor suppressor miRNA by inhibitors of DNA methylation and histone deacetylase may be a promising therapeutic strategy for HCC.

Key words: DNA methylation, epigenetics, hepatocellular carcinoma, histone modification, miRNA

INTRODUCTION

HEPATOCELLULAR CARCINOMA (HCC) is the most common type of liver cancer. Most cases of HCC occur secondary to either chronic hepatitis or hepatic cirrhosis caused by viral infection (hepatitis B or C) or alcoholism. HCC accounts for 85–90% of all primary liver cancers and is one of the most lethal forms of cancer and has a high global prevalence.[1,2] The lethality of liver cancer may arise from its resistance to existing anticancer agents, a lack of biomarkers and underlying liver disease that limits the use of chemotherapeutic drugs. In addition, the molecular pathogenesis of HCC remains poorly understood.

Epigenetics is an acquired modification of methylation and/or acetylation of chromatin DNA or histone proteins, which regulates downstream gene expression. Epigenetic alterations can be induced by aging, chronic inflammation or viral infection, and epigenetic aberrations may induce inactivation of tumor suppressor genes and play critical roles in the initiation and progression of human cancer.[3] Chromatin-modifying drugs such as DNA methylation inhibitors and histone deacetylase (HDAC) inhibitors have shown clinical promise for cancer therapy. The DNA methylation inhibitor 5-aza-2′-deoxycytidine (5-Aza-CdR) and the HDAC inhibitor suberoylanilide hydroxamic acid (SAHA) have emerged as promising agents for epigenetic therapy of human malignancies.[4]

We have been interested in sodium butyrate (SB), which was first demonstrated to suppress histone deacetylation *in vivo* and *in vitro* in 1977.[5] It has been shown then the activity of SB resulted from inhibition of HDAC activity.[6] Butyrate is an important substrate for maintenance of colonic health, and oligofructose fermentation by human fecal bacteria can increase butyrate production.[7] If several malignant phenotypes of HCC were induced by epigenetic process, epigenetic treatment may be possible to reverse malignant nature of HCC into normal nature because epigenetic change is reversible. We focused on the action of SB, which has been demonstrated to induce differentiation in a human

Correspondence: Dr Hidetsugu Saito, Division of Pharmacotherapeutics, Faculty of Pharmacy, Keio University, 1-5-30 Shibakoen, Minato-ku, Tokyo 105-8512, Japan. Email: hsaito@a2.keio.jp

Received 8 March 2013; revision 12 April 2013; accepted 21 April 2013.

colonic cancer cell line[8,9] and in human promyelocytic leukemia,[10] and has been utilized in clinical therapy.[11]

We first described the effect of SB on human HCC cell lines, PLC/PRF/5, HCC-M and HCC-T.[12] SB reduced the expression of *c-myc* and *c-fos* and induced normal or mature phenotype of hepatocytes in these cancer cells from transcriptional changes in α-fetoprotein (AFP) and albumin. We interpreted this change as evidence of liver cancer cell differentiation, because epigenetic alterations frequently occur during cellular differentiation in any cell types[13] and it has always coordinated with decrease in several malignant characteristics.[14–16] SB induced morphological changes in PLC/PRF/5 cells[17] and led to changes in antigens on the cell surface,[18] which led to further changes in the sensitivity to lymphocyte-activated killer cell attack.[19] In the early stage of the SB-induced phenotypic change, we found that upregulation of *bcl-2* and *mcl-1* peaked at 4–12 h after treatment with SB and that the upregulation was essential for the mechanism of anti-apoptosis in this system.[20] The same finding was also demonstrated in a reverse-side experiment showing that overexpression of *bcl-2* prevented human liver cancer cells from SB-induced apoptosis. SB caused cell-cycle arrest in the G1 phase via an increase in p21/WAF1 expression but this change was not associated with the p53 increase.[21] We also examined the effect of artificially decreasing *c-myc*, which had been increased through SB treatment, by transfecting an antisense oligodeoxynucleotide (ODN) against *c-myc* into human liver cancer cells, PLC/PRF/5, HCC-M and HCC-T. The antisense *c-myc* ODN inhibited cell proliferation with reduction of the G1 cell number and AFP expression, and increased the expression of albumin and human liver-specific antigen. These phenotypic changes were very similar to those induced by SB treatment.[22,23] It was interesting that the SB-induced cell phenotype of human liver cancer cells showed a less malignant phenotype. It has been suggested that SB reduced not only the chance of cell detachment from the same cell type by increasing the expression of cell-to-cell adhesion molecules, such as E-cadherin and β-catenin,[24] but also cell migration and mobility.[25] These changes were demonstrated to occur as a result of reduced expression of a small G-protein. It was further demonstrated that SB treatment reduced telomerase activity in cancer cells.[26] Thus, SB significantly reduced the malignant phenotype of human liver cancer cells, and it was thought that this change was induced by its action as an HDAC inhibitor. We investigated the comprehensive expression of mRNA in human liver cancer cells treated with SB, and found that some cross-talk occurred between the gene expression pathways induced by SB and interferon treatment.[27] Clinical aspects of HCC have also indicated that dedifferentiation occurs during malignant progression of HCC,[28,29] and it has been described as multistep hepatocarcinogenesis. The change during progression to malignant characteristics has been recently utilized in imaging diagnosis.[30,31]

Recently, we and other groups have revealed that epigenetic alterations regulate not only protein-coding genes but also non-coding genes such as microRNA (miRNA).[32] miRNA are small non-coding RNA that function as endogenous silencers of numerous target genes. Hundreds of miRNA have been identified in the human genome. miRNA are expressed in a tissue-specific manner and play important roles in cell proliferation, apoptosis and differentiation.[33,34] miRNA expression profiles can be used to classify the developmental lineages and differentiation stages of tumors. Interestingly, miRNA expression profiles are more accurate for tumor classification than conventional mRNA profiling.[35] Furthermore, recent studies have demonstrated the association of miRNA expression signatures with prognostic and disease progression factors in human malignancies.[36] Specific miRNA may be a powerful clinical tool for diagnosis and prognosis and as a therapeutic target for malignancies. Aberrant expression of miRNA may contribute to the development and progression of HCC.[37]

It has been thought that epigenetic therapy potentially changes malignant cells into a normal phenotype. This potential mechanism together with the recent discovery of miRNA prompted us to analyze the relationship between epigenetics and miRNA in relation to HCC, which is the focus of the present review.

ALTERATION OF DNA METHYLATION IN HCC

EPIGENETIC ALTERATIONS SUCH as DNA methylation and histone modification play critical roles in chromatin remodeling and regulation of gene expression in mammalian development and in human diseases.[38] Alteration of DNA methylation is one of the most consistent epigenetic changes in human cancers.[3] DNA methylation patterns are generated and heritably maintained by three active DNA methyltransferases, DNMT1, DNMT3A and DNMT3B. The de novo methyltransferases DNMT3A and DNMT3B act independently of replication and show equal preference for both unmethylated and hemimethylated DNA, whereas the maintenance DNA methyltransferase DNMT1 acts during replication and preferentially methylates hemimethylated DNA.[39]

DNA hypermethylation refers principally to the gain of methylation at specific sites that are unmethylated under normal conditions. This aberrant methylation occurs mainly in short CpG-rich DNA stretches called "CpG islands". DNA methylation can lead to gene silencing by either preventing or promoting the recruitment of regulatory proteins to DNA. Alternatively, it can provide binding sites for methyl-binding domain proteins, which can mediate gene repression through interactions with HDAC. This phenomenon of aberrant promoter CpG island hypermethylation has been associated with the stabilization of transcriptional repression and loss of gene function, and occurs fundamentally in tumor suppressor genes. In contrast, DNA hypomethylation is associated mainly with the loss of DNA methylation in genome-wide regions. DNA hypomethylation has been reported in several tumor types, such as colorectal and gastric cancers. DNA hypomethylation occurs in many gene-poor genomic areas, including repetitive elements, retrotransposons and introns, where it leads to genomic instability.[40]

To evaluate the significance of alterations in DNA methylation during human hepatocarcinogenesis, we have previously examined expression levels of DNA methyltransferases and DNA methylation status in HCC. Significant overexpression of DNMT1, DNMT3A and DNMT3B was observed in HCC compared with the corresponding non-cancerous liver tissues. DNA hypermethylation on CpG islands of p16 and methylated-in-tumor (MINT)1, 2, 12 and 31, and DNA hypomethylation on pericentromeric satellite regions satellites 2 and 3 were detected in HCC. Thus, aberrant expression of DNA methyltransferases and aberrant DNA methylation status on CpG islands and pericentromeric satellite regions play critical roles during human hepatocarcinogenesis.[41] We have also reported that the incidence of increased DNMT1 protein expression in HCC correlated significantly with poor tumor differentiation and portal vein involvement. Moreover, the recurrence-free and overall survival rates of patients with HCC exhibiting increased DNMT1 protein expression were significantly lower than those of patients with HCC that did not exhibit increased expression. Increased DNMT1 protein expression may play a critical role in the malignant progression of HCC and be a biologic predictor of both HCC recurrence and a poor prognosis in HCC patients.[42] DNMT3B is required for methylation on pericentromeric satellite regions during mouse development.[43] To clarify the molecular mechanism underlying DNA hypomethylation on pericentromeric satellite regions during human hepatocarcinogenesis, we examined mutations of the DNMT3B gene and expression levels of splice variants of DNMT3B in HCC cases. Mutation of the DNMT3B gene was not found in HCC. Overexpression of DNMT3B4, a splice variant of DNMT3B lacking conserved methyltransferase motifs IX and X, significantly correlated with DNA hypomethylation on pericentromeric satellite regions in HCC cases. These results suggest that overexpression of DNMT3B4, which may lack DNA methyltransferase activity, results in DNA hypomethylation on pericentromeric satellite regions accompanied by chromosomal instability in human hepatocarcinogenesis.[44]

ALTERATION OF HISTONE MODIFICATIONS IN HCC

THE N-TERMINAL TAILS of histones can undergo a variety of post-translational modifications including methylation and acetylation on specific residues. These histone modifications regulate transcription of genes which play important roles in cellular processes. Unlike DNA methylation, histone modifications can lead to either activation or repression depending upon which residues are modified and the type of modifications present. For example, tri-methylation of lysine 4 on histone H3 (H3K4me3) is enriched at transcriptionally active gene promoters,[45] whereas di- and tri-methylation of H3K9 and tri-methylation of H3K27 is present at gene promoters that are transcriptionally repressed.[46,47]

As shown in Figure 1, transcriptionally active chromatin in normal cells is characterized by acetylation of histone H3 and tri-methylation of H3K4. Epigenetic silencing of tumor suppressor genes during carcinogenesis is generally mediated by two distinct histone modifications: methylation of H3K9 and tri-methylation of H3K27. The polycomb repressive complex 2 (PRC2) mediates epigenetic gene silencing by tri-methylating H3K27. Methylation of H3K9 works in concert with DNA methylation, whereas tri-methylation of H3K27 occurs independently of DNA methylation.[48] HDAC induces deacetylation of histone H3 in both of these pathways of epigenetic silencing.

Recent studies have demonstrated that histone tails are aberrantly modified during human hepatocarcinogenesis. The level of H3K27 tri-methylation was significantly increased in HCC tissues relative to adjacent non-tumorous liver tissues. The increased level of H3K27 tri-methylation in HCC was significantly correlated with large tumor size, poor differentiation, advanced clinical stage, vascular invasion and shortened survival time of patients with HCC. These findings

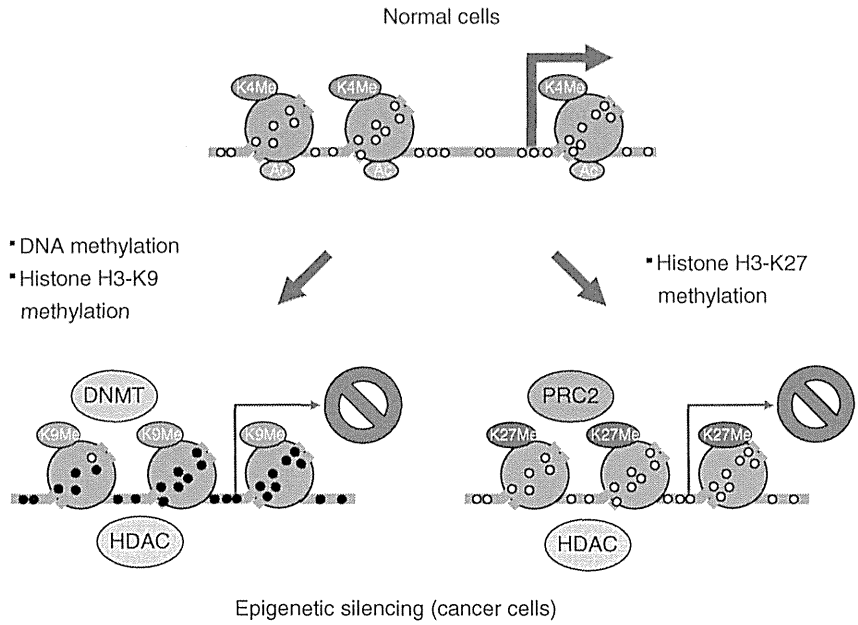

Figure 1 Epigenetic gene silencing in cancer cells. Transcriptionally active chromatin in normal cells is characterized by acetylation of histone H3 (Ac) and tri-methylation of H3K4 (K4Me). Epigenetic silencing of tumor suppressor genes during carcinogenesis is generally mediated by two distinct histone modifications: methylation of H3K9 (K9Me) and tri-methylation of H3K27 (K27Me). Polycomb repressive complex 2 (PRC2) mediates epigenetic gene silencing by tri-methylating H3K27. Methylation of H3K9 works in concert with DNA methylation induced by DNA methyltransferase (DNMT), whereas tri-methylation of H3K27 works independent of DNA methylation. Histone deacetylase (HDAC) induces deacetylation of histone H3 in the both pathways of epigenetic silencing. Open circle, unmethylated DNA; filled circle, methylated DNA.

suggest that a high level of H3K27 tri-methylation is an independent molecular marker for a poor prognosis in patients with HCC.[49] In addition, there are several reports demonstrating that enhancer of zeste homolog 2 (EZH2), which is a member of the polycomb group-protein family and a catalytic subunit of PRC2, was overexpressed in HCC.[14,50]

Yao and colleagues investigated histone modifications at the promoter regions of p16 (INK4a) during differentiation of embryonic stem cell–hepatoma hybrid cells. Tri-methylation of H3K27 at the p16 (INK4a) promoter region, occurring in the early onset of p16 (INK4a) silencing, was followed by di-methylation of H3K9 at later stages. During the induced differentiation of hepatomas, di- and tri-methylation of H3K4 were maintained at high levels during the silencing of p16 (INK4a), suggesting that H3K4 methylation events did not cause the silencing of p16 (INK4a). These findings indicated that the enrichment of tri-methylation of H3K27, independent of H3K9 methylation and DNA methylation, was an early event in the silencing of p16 (INK4a) during the tumor development. This histone modification pattern may be a heritable marker for epigenetic silencing of p16 (INK4a) during the developmental of HCC.[51]

It has been shown that high expression levels of class I HDAC correlate with a malignant phenotype and poor prognosis in human cancers. Wu and associates investigated the expression patterns and clinical significance of class I HDAC isoforms in a cohort of 43 hepatitis B virus (HBV)-associated HCC patients treated by liver transplantation. Class I HDAC were highly expressed in a subset of HCC with positivity for HDAC1 in 51.2%, HDAC2 in 48.8% and HDAC3 in 32.6% of cases. High expression levels of HDAC2 and HDAC3 were significantly associated with reduced recurrence-free survival of patients with HCC. HDAC3 in particular can be an independent prognostic factor. *In vitro* experiments with selective knockdown of HDAC isoforms by siRNA revealed that inhibition of HDAC2 and HDAC3, but not HDAC1, suppressed proliferation and the invasiveness of liver cancer cells. These findings demonstrate that HDAC3 plays a significant role in regulating tumor cell proliferation and invasion, and it could serve as a

candidate biomarker for predicting the recurrence of HBV-associated HCC following liver transplantation and as a potential therapeutic target.[52]

BIOGENESIS OF MIRNA

MIRNA ARE APPROXIMATELY 22 nucleotide (nt) non-coding RNA that can post-transcriptionally downregulate the expression of various target genes. Currently, approximately 1500 human miRNA have been identified in the human genome, each of which potentially controls hundreds of target genes. As shown in Figure 2, miRNA genes are generally transcribed from transcription start sites (TSS) by RNA polymerase II (pol II) to form primary transcripts (pri-miRNA). Pol II-transcribed pri-miRNA are capped with 7-methylguanosine and are polyadenylated. The nuclear RNase III enzyme Drosha and its co-factor DGCR8 process pri-miRNA into approximately 60-nt precursor miRNA (pre-miRNA), which form an imperfect stem-loop structure. Pre-miRNA are transported into the cytoplasm by exportin 5 and are subsequently cleaved by Dicer into mature miRNA, which are then loaded into the RNA-induced silencing complex (RISC). The miRNA/RISC complex downregulates specific gene products by translational repression via binding to partially complementary sequences in the 3′-untranslated regions (3′-UTR) of the target mRNA or by directing mRNA degradation via binding to perfectly complementary sequences.[53] miRNA are expressed in a tissue-specific manner and play important roles in cell proliferation, apoptosis and differentiation during mammalian development. Links between miRNA and the development of human malignancies are becoming increasingly apparent.[36,54,55]

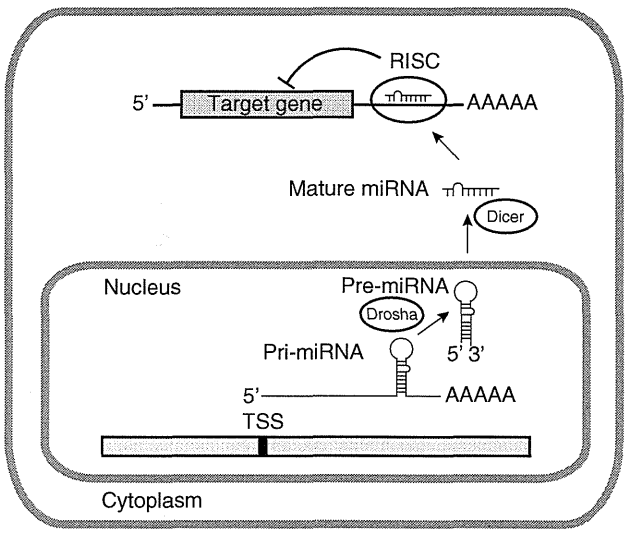

Figure 2 Biogenesis of miRNA. miRNA genes are transcribed from TSS by RNA pol II to form pri-miRNA which are capped with 7-methylguanosine and polyadenylated (AAAAA). Drosha and its co-factor DGCR8 process pri-miRNA into pre-miRNA. Pre-miRNA are transported into the cytoplasm and are subsequently cleaved by Dicer into mature miRNA. Mature miRNA are then loaded into RNA-induced silencing complex (RISC), where miRNA downregulate specific gene products by translational repression via binding to partially complementary sequences in the 3′-untranslated region of the target mRNA or by directing mRNA degradation via binding to perfectly complementary sequences.

PUTATIVE TUMOR SUPPRESSOR AND ONCOGENIC MIRNA IN HCC

SOME MIRNA ARE overexpressed in HCC, indicating that they may have roles as oncogenes accelerating the development of HCC. On the other hand, some miRNA are downregulated in HCC, suggesting that they may act as tumor suppressors. Aberrant expression of miRNA playing important roles in cell proliferation may contribute to the initiation and progression of HCC.

miR-122 is specifically expressed and highly abundant in the human liver. Recent studies have reported that *miR-122* may modulate and facilitate replication of hepatitis C virus, indicating that *miR-122* is a potential target for antiviral intervention.[56] *miR-122* can modulate expression of cyclin G1 as its target in HCC cells. In patients with HCC, lower *miR-122* levels were associated with a shorter time to recurrence, whereas higher cyclin G1 expression was related to a lower survival rate, suggesting that *miR-122* is a potential tumor suppressor miRNA in HCC.[57] *miR-122* also modulates Bcl-w expression by directly targeting the binding site within the 3′-UTR. The cellular mRNA and protein levels of Bcl-w were repressed by elevated levels of *miR-122*, which subsequently led to reduction of cell viability and activation of caspase-3. Thus, Bcl-w is a direct target of *miR-122* that functions as an endogenous apoptosis enhancer in HCC cells.[58,59] Distintegrin, metalloprotease family 10 (ADAM10), serum response factor (SRF) and insulin-like growth factor 1 receptor (Igf1R), which promote tumorigenesis, were validated as targets of *miR-122*. ADAM10, SRF, and Igf1R were upregulated in primary human HCC compared with non-cancerous tissue from the same patient liver tissue, suggesting that the loss of multifunctional *miR-122* contributes to the malignant phenotype of HCC cells.[60] Tsai and coworkers have